INSTITUTO SUPERIOR DE ENGENHARIA DO PORTO
MESTRADO EM ENGENHARIA MECÂNICA




Produção de Componentes Metálicos usando uma nova tecnologia de Manufatura Aditiva baseada em Arco de Plasma

JOÃO FRANCISCO ISIDORO
outubro de 2022

POLITÉCNICO
DO PORTO

Instituto Superior de Engenharia do Porto

PRODUCTION OF METALLIC COMPONENTS USING A NEW AM ARC-BASED TECHNOLOGY

João Francisco Isidoro

1170493

2021/2022

Instituto Superior de Engenharia do Porto

Mechanical Engineering

POLITÉCNICO DO PORTO

Instituto Superior de Engenharia do Porto

PRODUCTION OF METALLIC COMPONENTS USING A NEW AM ARC-BASED TECHNOLOGY

João Francisco Isidoro

1170493

Thesis submitted to Instituto Superior de Engenharia do Porto to comply with the requirements to obtain the degree of Master of Science in Mechanical Engineering, conducted under the supervision of Prof. Dr. António Gonçalves Magalhães

2021/2022

Instituto Superior de Engenharia do Porto

Mechanical Engineering

POLITÉCNICO DO PORTO

JURY

Chairman

Professor João Francisco Machado Gomes da Silva

Coordinating Professor, Department of Mechanical Engineering of ISEP

Main Supervisor

Professor António Gonçalves Magalhães

Coordinating Professor, Department of Mechanical Engineering of ISEP

Co-Supervisor

Professor Púria Esfandiari

Invited Professor, Department of Mechanical Engineering of ISEP

Arguer

Professor Fernando Jorge Lino Alves

Associate Professor, Department of Mechanical Engineering and Industrial Management of FEUP

ACKNOWLEDGEMENTS

First of all, I want to thank the most important people in my life, my parents, Isabel and Fernando, my brother, André and my girlfriend, Inês.

I would like to give special thanks to my supervisor, Professor Doctor António Gonçalves Magalhães, who accepted to be my supervisor, and that was always available, transmitting me the knowledge I needed to successfully complete this dissertation.

I also thank to my co-supervisor, Professor Púria Esfandiari for all the help in the various stages of this work.

I thank the community of the Department of Mechanical Engineering of ISEP, especially to the teachers and technicians of the laboratories for all the support provided whenever necessary. Namely, Professors João Silva and Arnaldo Pinto, and the Engineers Vítor Ribeiro, Vítor Moreira, Fátima Andrade.

I thank all the professionals of the Centre for Rapid and Sustainable Product Development (CDRSP), in particular Engineer António Raimundo da Silva, Pedro Sereno and Olivier Gouveia for making it possible to carry out this work and whose I had the opportunity to work with.

Finally, I would like to thank all my friends who accompanied me throughout this journey, Carlos Misael, Cristofe Fernandes, Tiago Barreira, José Ferreira and Tomás Almeida and my research colleagues João Carneiro, Manuel Soares and David Povoa.

I would also like to thank Agência Nacional de Inovação (ANI), for the project Metal.BOT that allowed financial support to carry the works developed in this dissertation.

Keywords

3DPMD, Eutroloy 16604, Additive Manufacturing, Plasma Transferred Arc, Powder Deposition

ABSTRACT

Additive manufacturing processes use a wide range of technologies and are increasingly used in several industries, abandoning the stigma that associates them exclusively with the manufacture of prototypes. Due to the advantages presented by this kind of process, such as the absence of moulds and a greater design freedom, additive manufacturing techniques have been incorporated in some industrial sectors.

These techniques of additive deposition can be divided into two main categories, namely the Powder Bed System (PBS) and the Direct Energy Deposition (DED). The PBS have been mostly implemented commercially, however present some disadvantages when compared to the DED, such as the limitation of the build volumes, lower production rates and greater difficulty in producing multi-material parts.

A new additive manufacturing technique called 3D Plasma Metal Deposition (3DPMD), which is part of the DED techniques, consists in the combination of Plasma Transferred Arc (PTA) welding technology with deposition by means of a robotic arm. This technology has been implemented due to its versatility, being applied for example in industries such as repair and coating of metal parts, or even in the mould industry.

In this dissertation, this additive manufacturing process, the 3DPMD, was used as an object of study in the possibility of manufacturing metallic parts, as well as repair processes. In this way, a study of the influence of various parameters of material addition in the process was performed, such as current intensity, speed and deposition rates, and then a qualitative analysis of the material produced was performed.

Using a PTA material deposition equipment, combined with a CNC equipment using CAM routines, process parameters were established according to the full factorial Design of Experiments (DoE). Thus, deposited beads were produced with the different parameters and submitted to hardness and geometric analysis tests, to evaluate the optimum process conditions.

The ANOVA test allowed concluding the inexistence of correlation between factors, while Spearmen's correlation coefficient allowed knowing the influence of each factor on geometry and hardness. Based on the results obtained, it was possible to produce a

piece by adding layers of metallic cord, creating a test cube, which was also submitted to Microhardness tests.

Palavras-Chave

3DPMD, Eutroloy 16604, Fabricação Aditiva, Arco de Plasma Transferido, Deposição de Pó

RESUMO

Os processos de fabricação aditiva recorrem a uma vasta gama de tecnologias, sendo cada vez mais utilizados em diversas indústrias, abandonando o estigma que os associa exclusivamente ao fabrico de protótipos. Pelas vantagens apresentadas por este tipo de processo, como por exemplo a inexistência de moldes e uma maior liberdade no projeto de peças, as técnicas de fabricação aditiva têm vindo a ser incorporadas em alguns setores industriais.

Estas técnicas de deposição aditiva, podem dividir-se em duas principais categorias, nomeadamente os de *Powder Bed System* (PBS) e os *Direct Energy Deposition* (DED). Os PBS têm vindo a ser maioritariamente implementados comercialmente, contudo com algumas desvantagens quando comparados com os DED, como por exemplo a limitação do volume das peças a fabricar, menores cadências de produção e a maior dificuldade em produzir peças multimaterial.

Uma nova técnica de fabricação aditiva denominada de *3D Plasma Metal Deposition* (3DPMD), enquadrando-se nas técnicas DED, consiste na combinação da tecnologia de soldadura por Arco de Plasma Transferido (PTA) com a deposição através de um braço robótico. Esta tecnologia tem vindo a ser implementada pela versatilidade que apresenta, sendo aplicada por exemplo em indústrias como a de reparação e revestimento de peças metálicas, ou mesmo na indústria de moldes.

Nesta dissertação recorreu-se a este processo de fabricação aditiva, o 3DPMD, como objeto de estudo na possibilidade de fabricação de peças metálicas, assim como processos de reparação. Desta forma, realizou-se um estudo da influência de diversos parâmetros de adição de material no processo, como por exemplo a intensidade de corrente, a velocidade e taxas de deposição, e seguidamente foi realizada uma análise qualitativa do material produzido.

Utilizando-se um equipamento de deposição de material PTA, combinado com um equipamento CNC utilizando técnicas CAM, foram estabelecidos parâmetros de processo de acordo com o planeamento de experiências de fatorial completo (DoE). Assim, foram produzidos cordões com os diferentes parâmetros e submetidos a ensaios

de análise de dureza e geométrica, como forma de avaliar as condições ótimas de processo.

O teste ANOVA permitiu concluir a inexistência de correlação entre fatores, enquanto o coeficiente de correlação do *Spearmen* permitiu conhecer a influência de cada fator na geometria e na dureza. Com base nos resultados obtidos, foi possível produzir-se uma peça por adição de camadas de cordão metálico, criando um cubo de teste, que foi também submetido a ensaios de Microdureza.

PARTS OF THIS WORK THAT HAVE BEEN PUBLISHED

J. Isidoro, D. Póvoas, P. Esfandiari, J. F. Silva, and A. G. Magalhães, "Correlations between Process Parameters, Geometric Parameters and Microstructure of Fe-Co-Cr-Mo Parts Produced by 3DPMD" *Mater. Proc.*, vol. 8, no. 1, 2022, doi: 10.3390/materproc2022008085

ABBREVIATIONS AND SYMBOLS

Abbreviations

3D	Three-Dimensional
AM	Additive Manufacturing
AWJ	Abrasive Water Jet
CAD	Computer Aided Design
CMT	Cold Metal Transfer
DED	Direct Energy Deposition
DMLS	Direct Metal Laser Sintering
DoE	Design of Experiments
EBDM	Electron Beam Direct Manufacturing
EBM	Electron Beam Melting
FFE	Full Factorial Experiment
HAZ	Heated Afected Zone
ISEP	Instituto Superior de Engenharia do Porto
ISO	*International Organization for Standardization*
LENS	*Laser Engineered Net Shaping*
SLM	Selective Laser Melting
SLS	Selective Laser Sintering
UTS	Ultimate Tensile Strength
WAAM	Wire Arc Additive Manufacturing
YS	Yield Strength

Units

A	Amperes
cm^3	cubic centimeters
GPa	Giga Pascal
g	grams
g/min	grammes per minute
MPa	Mega Pascal
mm	Milimeter
mm/s	Milimeters per second
N	Newton

Symbols

%	Percentage
µ	Mi symbol
ρ	Ro symbol
p	p-value
r_s	Spearmen's Correlation Coefficient

GLOSSARY OF TERMS

Apparent Density	It's the mass of the powder divided by its apparent volume (uncompacted powders). It can be measured using the hall flow meter. Size distribution, shape of particles are the principal influencers of this density.
Bulk Density	It's the ratio of untapped powder mass by its volume. The interparticle voids volume contribution is also included in this density. The test available to determine this value is measure according to ASTM B212.
Density	It's defined as the quotient from mass by volume.
Material Utilization Ratio	$\chi = (m_{raw\_material}/m_{part})$ x 100 (%)
Spatter	Non desirable phenomenon that can occur in gas metal arc welding process, consisting in droplets of molten metallic or non-metallic material.
Tap Density	It's the ratio between the mass of the powder and the volume occupied by the powder after it has been taped, under standard conditions of tapping. This Density is an increased bulk density. The test available to determine this value is measure according to ASTM B527.
True Density	It's the quotient between the mass of a particle and his volume, excluding open and closed pores. It only considers pores in particles themselves.

LIST OF FIGURES

LIST OF TABLES

INDEX

INTRODUCTION

1 Introduction

1.1 Contextualization

In more recent times, a greater diversification of manufacturing processes has been noted due to technological advances. Although Additive Manufacturing (AM) processes are known to be relatively recent, their concept is not particularly new for production of prototypes, and for parts that are produced in small series. In the las decade, these technologies earned a lot of attention by being widely studied, due to the advantages it poses, such as design freedom, optimization of material distribution, different material combination, reduction of lead time and process cost. Nowadays, AM processes have an important role in several industries, such as the aerospace, biomedical, automotive, construction and others [1], [2].

The AM processes with metals can be classified according to the feeding system, namely the Powder Feed Systems (PFS) or Wire Feed Systems (WFS), by the aggregate state of the feedstock (Powder or Wire), by the energy source (Laser Beam, Electron Beam or Plasma/Electric Arc), or even by the build volume and the binding mechanism. The two main categories reported in the literature are Powder Bed Systems (PBS) and Direct Energy Deposition (DED) [3], [4].

The Powder Bed Systems (PBS) are currently the most used commercially. However, this beam-based methods have their limitations, such as the high demand of the powder quality (purity, grain size, degree of agglomeration), and the complex AM system components, result in an increasing of the process costs and limiting the spectrum of available materials. Another disadvantage is related to the limited volume of construction, which does not allow the production of big components such as turbine blades and valves. Additionally, the low build-up rate when compared to other processes, is also a disadvantage of this process[5]–[8].

By comparison, the Direct Energy Deposition (DED) processes have more advantages compared to PBS, such as the site-specific deposition and repair, higher deposition rates and the possibility of producing higher volume parts. The arc-based processes have an additional interest, with lower cost investment compared to the beam-based processes and lower complexity (possibility to adapt the welding process) [9], [10]. The arc-based processes are the predominant wire-based, however, the restricted availability of different types of wire consumables, the impossibility to create multi-material

structures using on heat source in-situ and the wire feed rate directly coupled to the heat input, limit this type of process [11], [12].

The 3D Metal Plasma Metal Deposition (3DPMD) is a new plasma deposition process that uses powder as raw material and posing itself as an interesting alternative to the existent DED process such as WAMM and LENS [13], [14].

The AM processes are characterized by a layered build-up, therefore, the stability of the build-up process, regarding the component geometry and the layer thickness is essential for its success [15]. Consequently, the key to producing parts without dimensional errors and with good mechanical properties is the exact knowledge of the relationship between predefined process parameters. In this way, this work sought to carry out a more in-depth study of the process and its main parameters.

There are a few studies that have been conducted in this field, however, none of them used the Eutroloy 16604, an alloy with potential use for 3DPMD process, and with excellent properties (heat, thermal shock, corrosion, and cracking resistance) [16].

1.2 Main Goals

The main objective of this work is the evaluation of the correlations between process parameters and the resultant geometry and hardness of the parts produced by 3DPMD. Another objective is the production of a test geometry (cube) and the study of the hardness variation.

To achieve the mentioned goals, the following tasks must be carried out:

- Analysis of the methods and materials for the process of material deposition, as well as the equipment used for this purpose.
- Deposition of weld beads with different parameters to evaluate the consistency of the deposed material.
- Preparation of samples of the deposed weld beads to evaluation of the hardness of the produced material.
- Geometrical analysis of the deposed material, to assess the geometrical stability of the deposed material.
- Production of a solid sample for the analysis of hardness from the top layers to the bottom.
- Analysis of results and conclusions

1.3 Methodology used

This work was guided by the following methodology:

- Study of the AM processes;

- Extensive study of the plasma transferred arc process, and its application to the additive manufacturing processes;
- Implementation of the 3DPMD setup;
- Analyse the characteristics of the powder supplied by the manufacturer;
- Planning the experiments through a full factorial design of experiments;
- Carrying out the deposition tests;
- Preparation of the specimens (cutting, mould embedding, sanding, polishing);
- Perform microscopic records and micro-hardness tests on the deposited beads;
- Collect and analyse the data using statistical tools, correlating the influence of each parameter on the process;
- Production of a test geometry (cube);
- Preparation of the cube (cutting, sanding, polishing);
- Perform microscopic records and micro-hardness tests on the cube cross-section;
- Preparation of this dissertation report;

1.4 Thesis Structure

The thesis is divided into four main chapters, whose content is summarised below:

Chapter 1

A brief contextualisation of the additive manufacturing of metals process is presented, focusing on the 3DPMD. The main objectives are also presented, the structure is described, and a summary is made of the topics covered in each chapter.

Chapter 2

This chapter presents the theoretical basis that allowed this work to be carried out. The AM processes, their particularities, their applicability, and their importance in the current industrial context are described. The results obtained in previous studies are also presented.

Chapter 3

The whole experimental procedure is described, and the respective results obtained are presented and analysed.

Chapter 4

The main conclusions of this work are presented and guidelines for future work are suggested.

STATE OF ART

2 State of Art

2.1 Additive Manufacturing of Metals

Additive Manufacturing (AM) includes all the techniques to produce components via material addition, by addition of layers of layers [17]. The most common ways to name additive technologies are: additive processes, layer manufacturing and freeform fabrication [18]. The ASTM F-42 committee defined AM as:

"The process of joining materials to make objects from 3D model data, usually layer upon layer, as opposed to subtractive manufacturing technologies"

Comparing to the conventional subtractive production (e.g: milling), in AM of metals, the components are produced layer by layer directly from 3D model (CAD data), using powder or wire as raw material, that is melton or fused by a heat source [19]. When it solidifies, produces the intended geometry according to the trajectory defined [20], [21]. The AM requires an innovative thinking of the design, while for the traditional manufacturing the design goal is to define which material will be removed, in AM the designer will decide which material will be added (Figure 1). Figure 2 presents a comparison between Traditional Manufacturing and Additive Manufacturing, this is presented by two charts, at left a unit cost versus production volume and at right a unit cost versus product complexity. The AM is indicated to low production volume and high complexity.

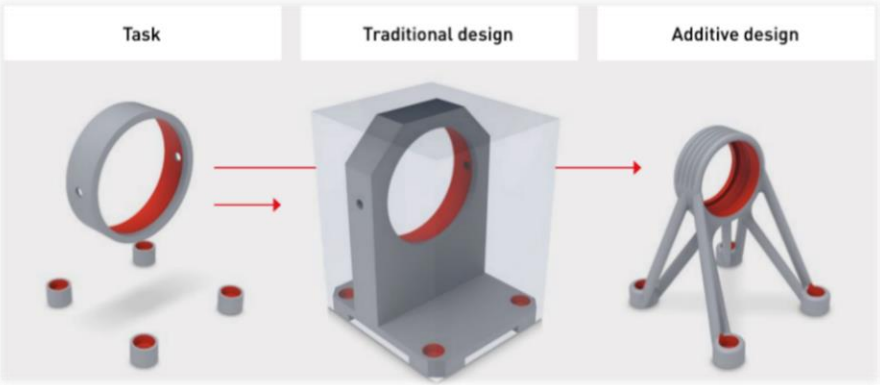

Figure 1 - Same task developed with Traditional vs Additive design [22]

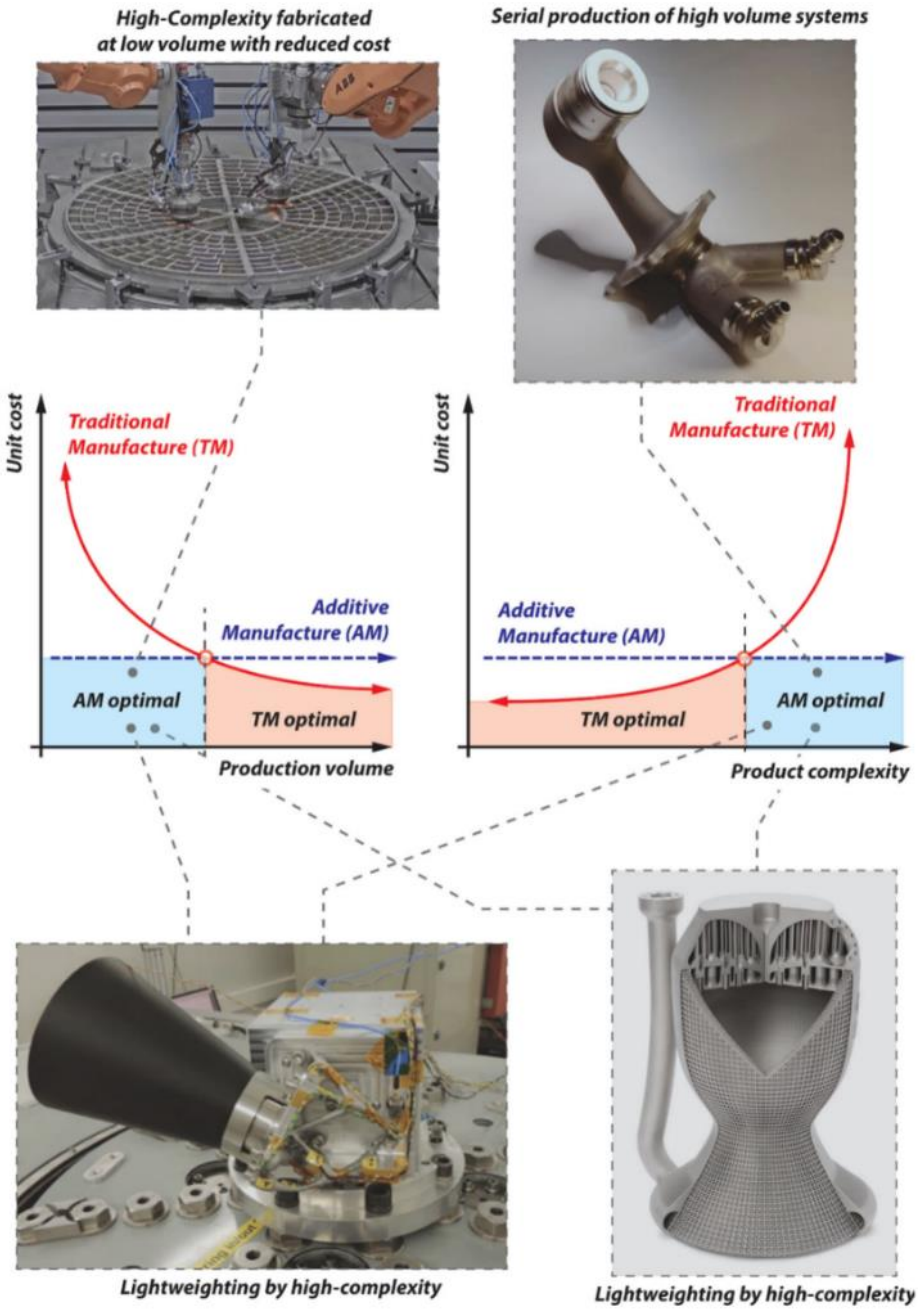

Figure 2 - On left, the graphic of unit cost versus production volume and on right unit cost versus product complexity [1]

AM earned considerable attention over the years due to its advantages, taking a significant role in several industries (aerospace, biomedical, automotive, construction and others) [23]. In Figure 3 are represented five different metallic parts (Bearing block,

turbine wheel, belt link, end cap and venturi), produce via two AM processes (EBM and DMLS).

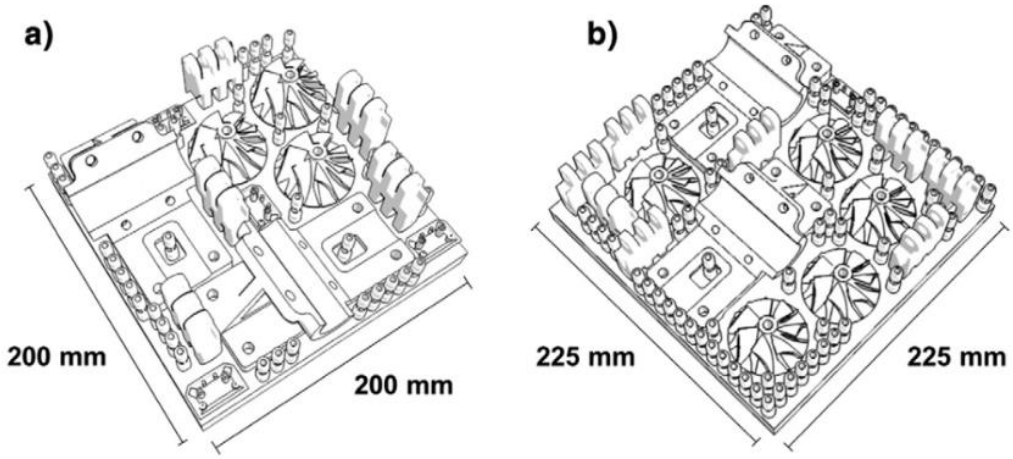

Figure 3 - Components produced via EBM (a) and DMLS (b) [24]

The main advantages of AM are the reduction of lead time and process cost, allowing a freedom of design and enabling to design and manufacture complex geometries with novel materials and unique design solutions [25]. These complex geometries can be improved, optimizing the material distribution, to reduce even more the mass while maintaining the mechanical properties [26]. It's also possible to combine different components, reducing potential failure modes, across joints and cost for multiple elements [27]. Furthermore, this technology has the possibility to recycle materials and reprocess. Finally compared to traditional manufacturing process, AM uses much less material by mass [1].

However, this process has its disadvantages: a limited range of materials that can be used, uncertainty of final material properties, post-processing requirements, the need of design skills that allows the design of complex products with less mass, rigorous quality control and certification [28].

The AM process can be classified according to the Feeding System (Powder Bed Systems, Powder Feed Systems or Wire Feed Systems), Feeding Stock/Aggregate State of the Feedstock (Powder or Wire), Energy Source (Laser Beam, Electron Beam or Plasma/Electric arc), Build Volume, Binding Mechanism (Solid State Sintering, Chemical Induced Binding, Liquid Phase Sintering Partial Melting, Full Melting) [18], [19], [29].

Although, different authors categorize in different ways the AM technologies, in this state of art, the processes are divided in two main categories, Powder Bed Systems (PBS) and Direct Energy Deposition (DED).

2.2 Powder Bed Systems (PBS)

PBS includes all the systems that use a high source of thermal energy (electron beam or laser beam) to melt (Powder Bed Fusion) or sintering (Powder Bed Sintering) the powder bed in defined regions, binding them to create the desired geometry, repeating the process, layer by layer, until the final component is done.

The most commons are Laser Beam Melting (LBM), commonly known as Selective Laser Melting (SLM), Direct Metal Laser Sintering (DMLS) and Electron Beam Melting (EBM) [30]–[32].

2.2.1 Selective Laser Melting (SLM)

The **SLM** was developed in 1999, by Dr. M. Fockele and Dr. D. Schwarze of F. & S. Stereolithographietechnik GmbH, with support of Dr. W. Meiners, Dr. K. Wissenbach, and Dr. G. Andres, from Fraunhofer Institute of Laser Technology. The first machines launched were Realizer 250 SLM and SLM Realizer 100. Since this release other companies explore this concept, bringing to the market other models, using the same principals [33].

In Figure 4 is represented a sequence of steps in this process. After the deposition of powder bed, a high-power fiber laser scans the powder's surface, melting the selective areas and bonding them. This process will repeat layer by layer as defined previously in the 3D model, until the building is complete. The final step is removing the powder that wasn't melted, reveling the final component. The SLM parts are produced in an inert gas atmosphere such as argon to remove oxygen from the building chamber [34].

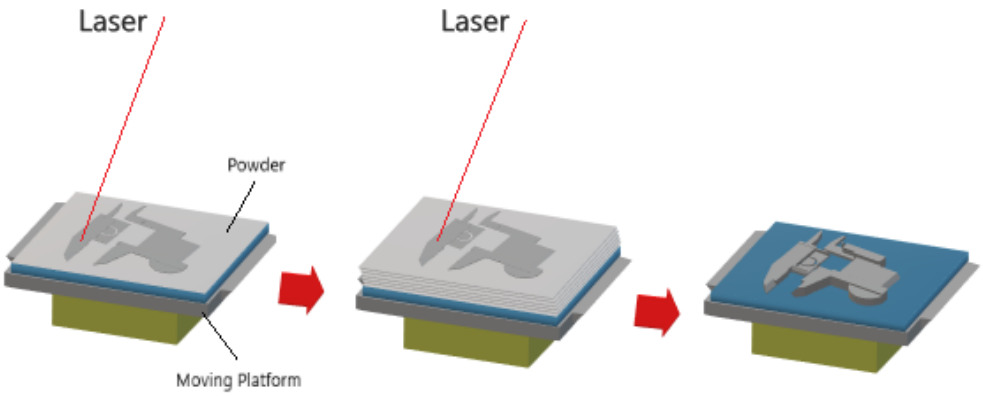

Figure 4 - Concept of SLM Process (adapted [33])

Figure 5 represents the principal components of these systems. This process uses a focused laser beam, the laser system is an EOS M270 that uses a YAG fiber laser with 100µm diameter (1), the number (2) is a CAD driven rotating mirror system that scans the laser beam and focus onto the powder bed (3). There is a mechanical recoated (4) that will form the powder layers on the build platform (5). The supply container (6) contains the powder which is continuously fed layer by layer onto the platform (5). In (7) is deposited the surplus powder to be recycled.

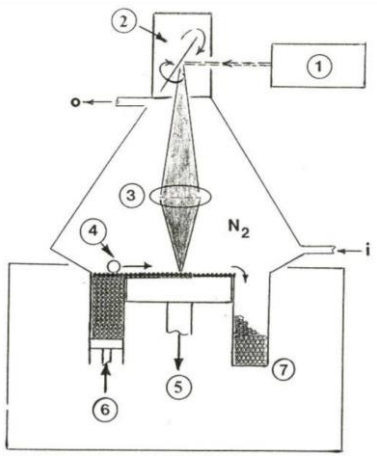

Figure 5 - Schematic representation of SLM [5]

2.2.2 Direct Meal Laser Sintering (DMLS)

The **DMLS** is based on a process called Selective Laser Sintering (SLS), however in this process it's used metallic powder. This process is similar to SLM, using a laser to scan specific areas on powder bed, repeating the process layer by layer, although the powder instead melted is sintered or partial sintered [34].

This process uses one or two metallic powders, in the second case one of the metal powders will serve as structural element (the one with highest melting point), and the other as bonding metal (the one with lowest melting point). The energy given by the laser has elevate the temperature of the powder to a medium melting temperature from the two metals [35].

One of the disadvantages of this process compared to traditional casts is the poor mechanical properties obtained, being necessary a postprocessing to form the final dense components. This post-processing stage can introduce stresses, that makes all process even more difficult to control [34].

2.2.3 Electron Beam Melting (EBM)

The **EBM** is a process very similar to the Laser Powder Bed Systems, with the difference that in this process it is used an electron beam as energy supply.

The main components of the machine are represented in Figure 6 - a. The gun (1) generates the electrons, and these are accelerated using electromagnetic lenses (2) to obtain a potential of 60kV. After that, the electrons are electromagnetically scanned by (3). The melt scan (3) melts only selected layer areas as prescribed in the CAD model. Powder contains in (4) fall to the build table (7) guided by a rake (5). The (6) goes down to each successive layer.

This system operates under a vacuum of <10-4 Torr. Helium gas is also injected into the chamber to increase the pressure (≈10-2 Torr). The chamber conditions improve the component's heating and cooling conditions, allowing to work with a large temperature spectrum (a large range of materials can be used), without affecting the produced components' mechanical properties [5], [6], [19].

a) **b)**

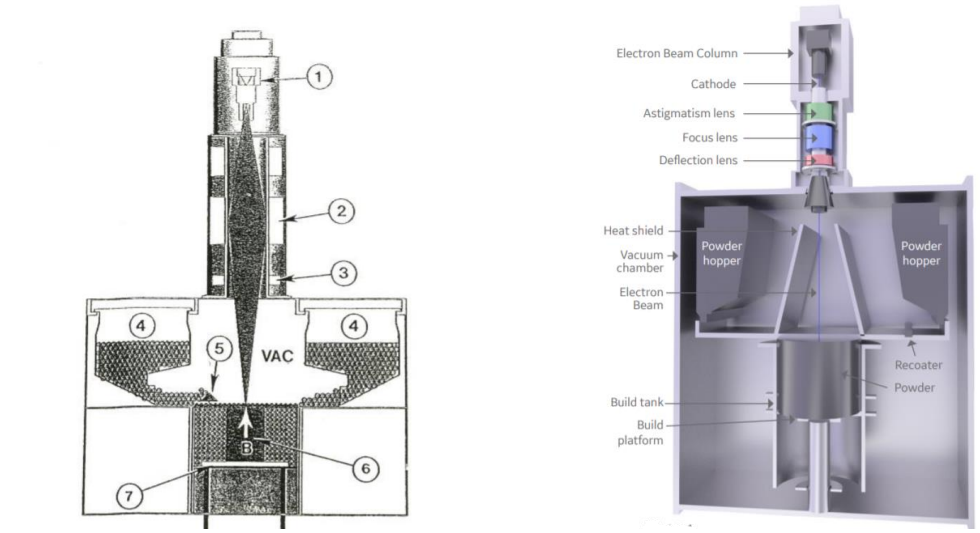

Figure 6 - EBM machine Representation [36], [37]

In Figure 6 – b it is represented (3) in more detail, in particular the electron beam column: the Cathode or Filament that generates the electrons and the electromagnetic lenses that are compounded by Astigmatism Lens, Focus Lens and Deflection Lens. This process is capable to produce metallic parts with high density and mechanical properties closer to the properties obtained via traditional processes, and it has a high energy efficiency (Figure 7), with highly reflective metals such as aluminum [38].

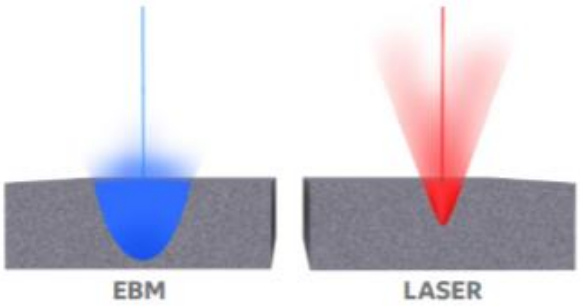

Figure 7 - Comparison between laser and electron beam penetrance [37]

2.2.4 Powder Bed Systems process parameters

The main process parameters of SLM and DMLS are Laser Power, Scanning Speed, Hatch Spacing and Layer Thickness.

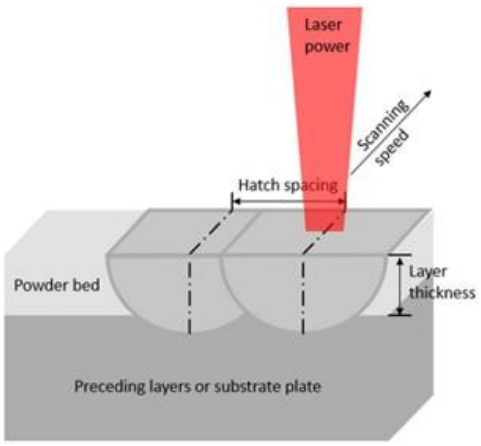

Figure 8 - SLM process parameters: Laser Power, Scanning Speed, Hatch Spacing, Layer Thickness [33]

To build consistent parts with almost full density is necessary to combine suitable parameters of scanning speed, v_s [mm/s], hatching space, h_s [mm], laser power, P_L [W], and layer thickness, D_s [mm] [33]. The volume energy, E_V [J/mm^3], can be calculated combining these parameters, according to the following equation:

$$\boldsymbol{E_v = \frac{P_L}{(v_s \cdot h_s \cdot D_s)}} \quad (1)$$

The typical values of these parameters found in literature [19], [22], [34], [39], for SLM process are D_s: 20 µm – 100 µm, P_L: 20 W – 1kW and v_s: up to 15 m/s.

In the EMB process the parameters are similar, except for the energy source. The typical values are D_s: 50 µm – 200 µm, High beam: 30mA and v_s: up to 10^4 mm/s.

2.2.5 Powder Deposition Techniques

In Powder Bed Process there are three main methods to deposit the powder layer (Figure 9).

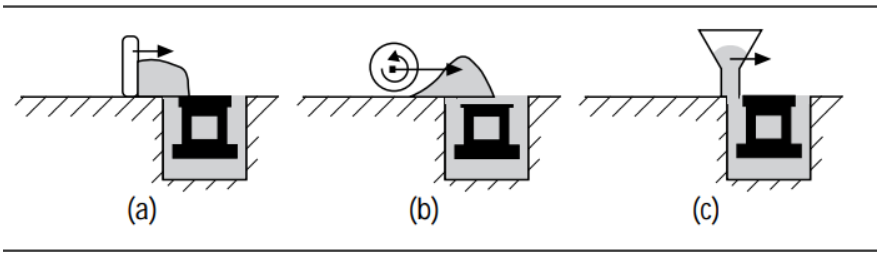

Figure 9 - Powder deposition methods: (a) scraper blade, (b) counter rolling cylinder and (c) slot feeder [39]

The type of deposition is crucial to the thickness of the layer and consequently the mechanical properties of the final product. The first one (a), presented in Figure 9, uses a scraper blade that will sweep the powder placed in front over the container. The main problem of this method is the lack of compaction after deposition. In Table 1, are represented different densities obtained according to the compaction, showing the big difference between apparent and tap density [40], [41].

Table 1 - Apparent, Tap and True Densities for different components, produced via different powders and mixture of powders, by Selective Metal Powder Sintering (SMS) (Adapted [39])

Powders	Dimension of Powder (µm)	Apparent Density (g/cm3)	Tap Density (g/cm3)	True Density (g/cm3)	Ratio Apparent/true (%)	Ratio Tap/true (%)
Cu	(25-40)	2.34	3.24	8.20	28.50	39.50
Fe	(63-80)	2.40	3.08	7.46	32.20	41.30
Fe-Cu1	(-)	2.64	3.91	7.71	34.20	50.70
Stainless Steel	(10-50)	4.55	5.37	7.82	58.20	68.70

[1]Fe + 30 percent Cu

The second deposition (b) process uses a rolling cylinder. This method eliminates the problem of contact line irregularities between cylinder and the powder surfaces and allows, the layer, to have a good compaction, leading to a tap density that produces better mechanical results in the final component produced.

The solutions (a) and (b) doesn't require high flow rates of the powders, however, the better the powders flow, the better will be the accuracy of the layer deposit.

The third deposition method (c), contrary to the other two, uses powders, with high flow rate, that are deposited into the container. An advantage from this process compared to the other two, is the reduction of friction to almost zero.

Another solution is a hybrid deposition (Figure 10), combining the advantages of roller cylinder for compaction, and the slot feed for deposition with minimum friction, leading to higher tap density.

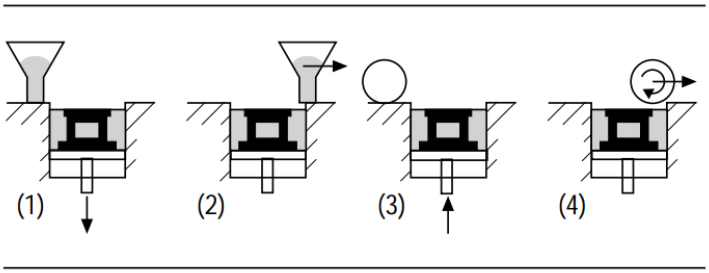

Figure 10 - Combine deposition mechanism (Slot feed deposition & Roller Cylinder Compaction [39]

2.2.6 Industrial Solutions

In Table 2 are represented different machine models of Laser powder-based machines presented on market, and the respective representation in Figure 11.

Table 2 - Different machine models of Laser Powder-Based Machines

Model	Company	Build Volume [mm]	Laser Power [W]	Technology	Ref.
M3 Linear	Concept Laser	300x350x300	200/400	Laser Melting	[42][43]
AM250	Renishw	250x250x300	200/400	Laser Melting	[44]
PXL	Phenix System Group	250x250x300	500	Laser Sintering	[45][46]
SLM250HL	SLM Solutions*	248x248x250	200/400	Laser Melting	[47]

*SLM Solution has another machine models

a) b) c) d)

Figure 11 - a) M3 Linear by Concept Laser [42] b) Phenix PXL by Phenix System Group [45] b) AM 250 by Renishaw [44] c) SLM 250HL by SLM Solutions GmbH [47]

In Table 3 are represented the properties of *Arcam EBM S12*, an EBM machine, and the respective representation in Figure 12.

Table 3 – Properties of an EBM machine

Model	Company	Build Volume [mm]	Beam Power [W]	Technology	Ref.
Arcam EBM S12	Arcam	200x200x180	3500	Electron Beam Melting	[48]

Figure 12 - Arcam S12 [48]

2.2.7 Experimental Results

The powder bed processes have been the subject of numerous studies, mainly for special applications, that by conventional subtractive manufacturing are unable to perform.

In Table 4 are presented a short resume of different properties obtained in previous studies via SLM and EBM compared to traditional manufacturing methods, using the same alloys. These processes show their ability to produce components with similar or even better mechanical properties, using post heat-treatments these properties can be adjusted.

Table 4 - Comparison of the results obtained by traditional processes and AM Powder Bed Process

Machine	Alloy	P [W]	v [mm/s]	H [J/mm]	Orient.	YS [MPa]	UTS [MPa]	Elong. [%]	Ref
Renishaw AM250	Ti-6Al-4V	157	225	0.70	Long. Transv.	978±5 967±10	1143±6 1117±7	11.8±0.5 8.9±0.4	[49]
Realizer PBF-L	Ti-6Al-4V	200	1000	0.20	Long. Transv.	1220 1200	1150 1300	6 6±1	[50]
EOS M270 SLM	Inconel 625	200	800-1200	0.25	Long.* Transv.*	380 360	900 880	58 58	[36]
Arcam A1	Ti-6Al-4V	50 - 3500	3000	0.70	Long. Transv.	783 ± 15 812 ± 12	833 ± 22 851 ± 19	2.7 ± 0.4 3.6 ± 0.9	[51]
Arcam A2	Ti-6Al-4V	7000	1000	7.0	Long. Transv.	1006 1001	1066 1073	15 11	[52]
Arcam A2	Inconel 625	1800	10,000	0.18	Transv. Transv.**	410 330	750 770	44 69	[36]
Casting	Ti-6Al-4V					862-999	934-1173	6-7	[53]
Casting	Inconel 625					318-380	587-665	25-30	[36]

*Heat-Treatment: HIP
**Heat-Treatment: Homogenization treatment (1080°C, 1.5h/air cooling) + Solution Treatment (980°C, 1h/air cooling) + double aging (720°C, 8hfurnance cooling + 620°C, 8h/air cooling)

2.3 Direct Energy Deposition (DED)

DED is a category of AM processes, that contrarily to PBS, that melt or sinter the material, which has been previously disposed in a layer, the material is melted or sintered while its being deposited. After the deposition process, the produced part is removed from the material base by machining and it's usually necessary a finishing operation to get the wanted surface quality [54].

However, the DED process involves a large range of different process, consequently the quality and properties of produced parts, depend on type of DED technology (type of feedstock and heat source), build environment (vacuum, inert gas, or ambient), deposition parameters (laser scan speed, laser power, hatch spacing, powder feed rate, laser scan strategy) [55].

In general, the main advantages of DED process compared to Powder Bed Process are [30], [32], [54], [56], [57]:

- Possibility to modify and repair a metal piece, after it's produced (coatings, fill cracks);
- Possibility to create Multi-Material Additive Manufacture (MMAM) and Functionally Gradient Structures;
- Almost unlimited assembly space;
- Higher deposition rates;
- Lower cost of raw material and low process complexity;
- Improved utilization factor of raw materials;

However, the disadvantages that can be found are:

- Often requires post machining finish (surface roughness);
- Shrinkage;
- Residual stress and deformation (due to temperature gradient);
- Lower dimensional resolution;
- Lower powder efficiency and recyclability.

DED processes can be denominated by Powder Feed System (PFS) or Wire Feed System (WFS) according to the raw material used, powder (Figure 13 – a) or wire (Figure 13 -b), respectively. In terms of the energy source, DED can be Beam-based (Laser or Electron) or Arc-based (Electric/Plasma Arc). The arc-based process born from welding technologies [34].

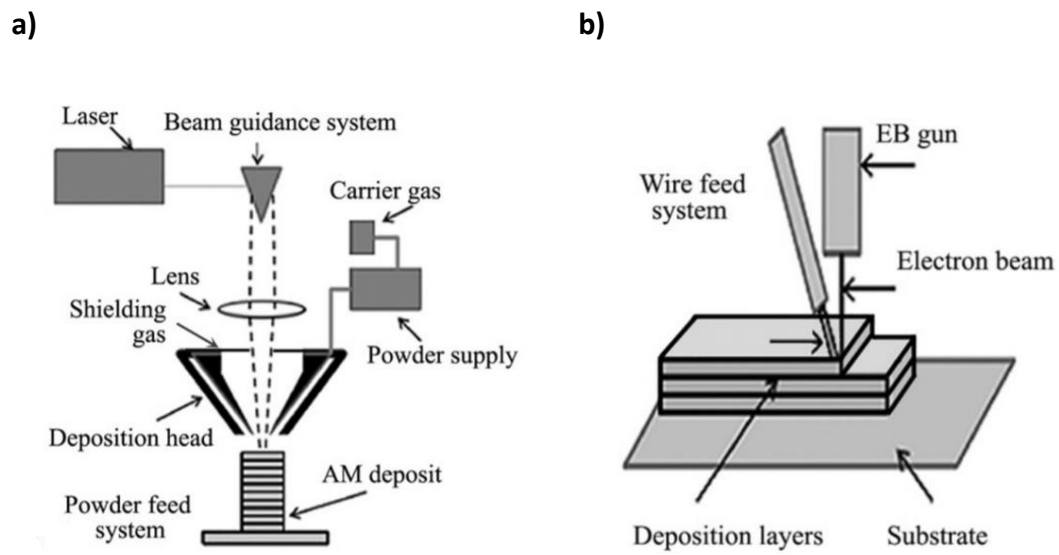

Figure 13 - a) Scheme of DED-L (LENS) b) Scheme of DED-EB (EBDM) system wire-fed [34]

In Table 5 it is represented a comparison between powder feedstock and wire feedstock process

Table 5 - Powder vs wire as raw material DED process (adapted [55])

Parameters	Powder	Wire
Deposition Rate	Draw	
Feedstock Material Variety	Lose	Win
Feedstock Material Cost	Lose	Win
Machine Cost	Draw[1]	
Safety	Lose	Win
Power Efficiency	Draw[2]	
Feedstock Capture Efficiency	Lose	Win[3]
Larger Parts Sizes	Lose	Win
Higher energy Input Required to melt Feedstock	Lose	Win
Lower Porosity	Lose	Win
Higher Resolution	Win	Lose
More Complex Geometry	Win	Lose
Surface Finish	Win	Lose
Dimensional Accuracy	Win	Lose

[1]In the case of Arc-Based Systems
[2]E-beam and arc systems have the high-power efficiency
[3]~ 100%

In Table 6 it is represented a comparison between DED process with different heat sources, 1 is the lowest and 4 the highest score. The build volume is referent to the relative size that components can be produced. Detail resolution it's the ability to create small features. Deposition rates refers to the rate that a product can be produced. Coupling efficiency, it's the efficiency of energy transfer from the energy source to the substrate. Potential for contamination as the name implies is the potential no add dirt, gas and other possible contaminants to the component.

Table 6 - Comparison between DED process with different heat sources [55]

Heat Source	Build Volume	Detail Resolution	Deposition Rate	Coupling Efficiency	Potential for Contamination
Laser	3	2	2	1	3
Electron Beam	4	1	3	4	4
Plasma/Electric arc	3	1	3	4	2

In Table 7 are represented the most common commercial denominations of the process according to the raw material and the energy source. The 3DPMD process was the process explored in more detail, in this review, because of his interest for practical work of the thesis.

Table 7 - Different commercial designation for AM process according to the energy source and raw material [18], [58]-[59]

Energy Source/Raw Material	Wire	Powder
Laser Beam	-	Laser Engineered Net Shaping (LENS)
Electron Beam	Direct Energy Deposition-Electron Beam (DED-EB) or Electron Beam Direct Melting (EBDM)	-
Plasma/Electric Arc	Wire Arc Additive Manufacturing (WAAM) Process (ex.Cold Metal Transfer - CMT)	3D Plasma Metal Deposition (3DPMD)

2.3.1 Laser Engineered Net Shaping (LENS)

LENS process is a DED technology developed by Sandia National Laboratories, and it was the first commercialized and trademarked. This process uses a laser as heat source to melt powder that is directly deposited in molten pool (Figure 14).

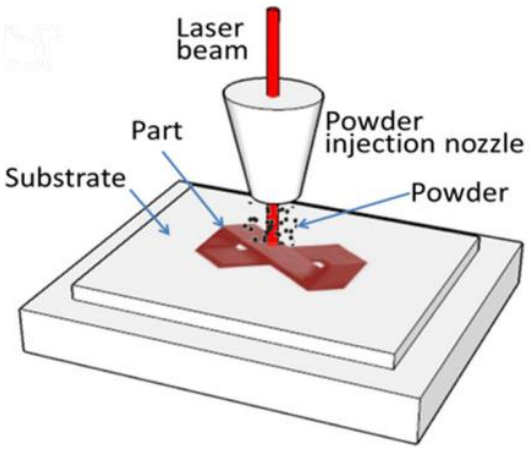

Figure 14 - Representation of LENS [60]

This process is very well known and studied, showing good results all over the years. Hanliang *et al.* [61] study the production of titanium parts via this process. The compositions of the structures manufactured where very similar, when compared to traditional technologies (Table 8). Post-deposition heat treatments can be performed to optimize the microstructure and improve the overall performance.

Table 8 - A comparison of chemical compositions of Ti– Nb– Zr– Mo– Sn alloy manufactured by LENS with conventionally processed materials, wt% (adapted [61])

Manufacturing Process	Ti	Nb	Zr	Mo	Sn	Other minor impurities
LENS	Bal.	20.9	3.09	1.90	1.7	>0.2
Casting	Bal.	25.1	3.08	2.90	2.02	>0.2
Cold Rolling	Bal.	25.0	2.75	2.82	1.80	>0.2

The Laser-based process, as such LENS, dominate the solutions used until now [62], however, the laser-based process requires high investment costs, laser protection system, and have medium deposition rates (20-150 cm^3/h). The arc-based process, in particular 3D Plasma Metal Deposition (3DPMD) closes this gaps, with relatively low investment costs, increased build-up rates (up to 1300cm^3/h), low demands on the powder characteristics, and also allow to mix powders (up to four), to obtain specific

local properties, according to the type and level of the loads the components are subjected [13],[15]-[63].

2.3.2 3D Plasma Metal Deposition (3DPMD)

The **3DPMD** is a new process based on a classical Plasma Transferred Arc (PTA) welding, and it uses a robot. The process initiates with the generation of the virtual slicing of CAD model into defined layers, them the robot path movement and the welding commands are programed based on the layer's information. Figure 15 represents an example of a 3DPMD setup.

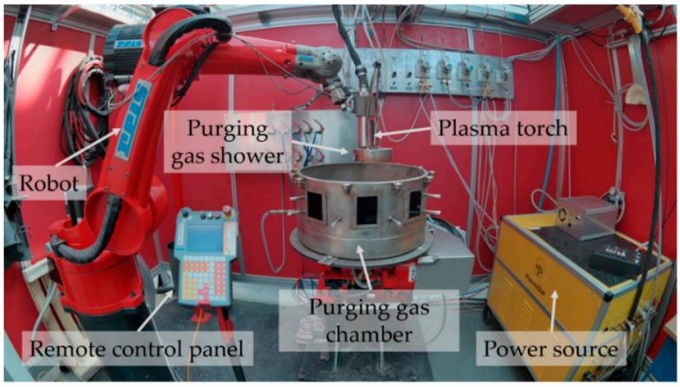

Figure 15 - Experimental setup for the robot based 3DPMD used in [62] to produce titanium parts

The PTA process is very similar to the conventional Plasma Arc Welding, however, in this process it's easier to control the plasma arc and the heat input, since the energy provided is practically all used to melt the metal. The heating of the base metal is minimum. Therefore, the heated affected zone (HAZ), distortions and dilution percentage are reduced. The typical dilution percentage for this process are in a range of 5 to 20%. The welding times are also short, and the requirement of post-weld machining is low [64]–[66].

In Figure 16 is represented the PTA process, which is composed by: (1) cathode holding device, (2) Plasma gas, (3) Cathode (tungsten), (4) Cooling water, (5) Shielding Gas, (6) Feeding gas (pressurized gas) and powder, (7) Welding direction, (8) Ignition, (9) Double power supply.

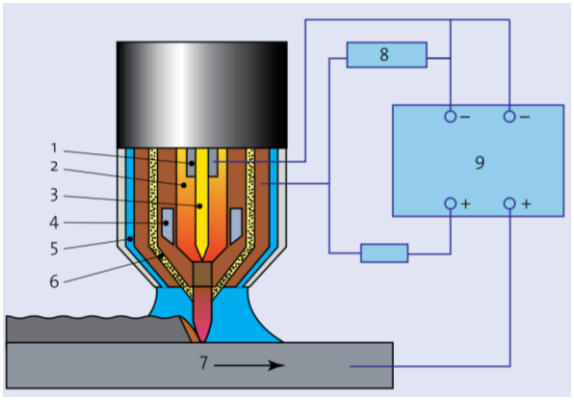

Figure 16 - Plasma Transferred Arc Welding [16]

In Figure 17 is represented the PTA process applied to a 3DPMD process. The process starts with the increase in the ionization of the gas by making the electric arc being compressed when passing through the heat resistant cathode to the workpiece. The resulting plasma arc (electric arc formed by ionized gas) has a high temperature and energy density. Then, the metallic powder is conveyed by a gas into the plasma arc column. A shield gas ensures the protection of the plasma arc column and the molten metal pool, from the surrounding air [67][68].

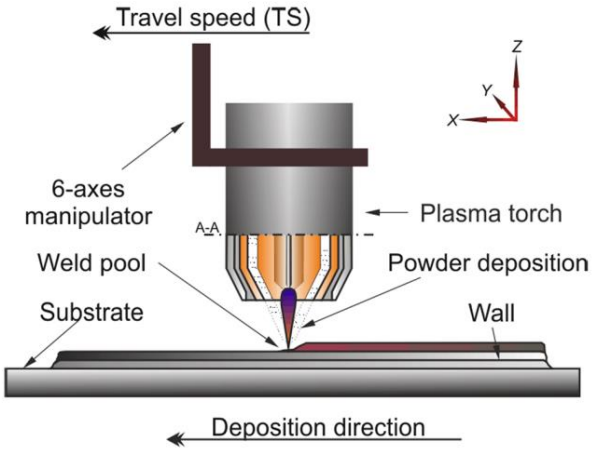

Figure 17 - Process setup for 3DPMD, in particular the plasma torch [69]

The energy input per unit/Heat Input, E [J/mm], can be calculated using Equation 2, being I [A] the welding current, U [V] the voltage, η [-] the efficiency and the and v [mm/min] the welding speed or weaving speed [70], [71]. Other important parameters of 3DPMD process are the powder flow rate and the gas parameters (type and amount).

$$E = \frac{U \cdot I \cdot \eta}{v} \quad (2)$$

The required amount of heat to the melting pool in J, Q_i, is given by the equation 3, where m_i is the supplied powder mass in g, c_i the heat capacity in J/kg·K, and ΔT_i the difference between final and initial temperature in K. Equation 4 describes how to calculate the m_i, being $\dot{m}_{P\_i}$ the powder feed rate in g/min and t_{si} the welding time in s.

$$\boldsymbol{Q_i = m_i \cdot c_i \cdot \Delta T_i} \quad (3)$$

$$\boldsymbol{m_i = \dot{m}_{P\_i} \cdot t_{si}} \quad (4)$$

AM processes are characterized by a layered build-up, therefore, the stability of the build-up process, regarding the component geometry and the layer thickness are essential for the success of manufacturing process. For example, in additive components that require a high number of layers (the most common situation), the slice distance per layer has a big importance. A deviation of 0.1 mm per layer with a number of 200 layers leads to an increase in the arc length from 10 mm to 30 mm, resulting in an arc voltage increasing (=higher heat input) continually due to the increased arc resistance. This unstable arc conditions cause the interruption of the process [70].

Thereby, Kevin [70] studied the correlations between process parameters (welding current, welding speed and powder mass flow) and geometric parameters (layer and wall Thickness) in manufacturing of weld seams from austenitic stainless-steel powder.

The conclusions obtain are pointed out:

- Welding current increase leads to layer thickness decrease and wall thickness increase;
- Welding speed increase leads to a parallel decrease in the layer and wall thickness;
- Variations on powder mass flow only affect the layer thickness.

Eva *et al.* [57] studied the correlations between process parameters to achive the best combination, producing weld seams from a Nickel-based alloy powder (Hastelloy C-22). The best combination was:

- Current: 180 [A]
- Travel Speed: 400 [mm/min]
- Feed Rate: 29.0 [g/min]

In this study, they also applied oscillation to the welding tests plate during deposition to improve the quality. The oscillation allows to the torch stay longer on the top of the heated spot after the weld pool. The oscillation parameters used:

- Amplitude: 7.5 [mm]
- Overlapping: 2.5 [mm]

The fabrication of a wall (120 x 40 x 15) was taken, using the base plate oscillation, and starting with the best combination of parameters for layer 1 and continuously decreasing the current and the feed rate and increasing the travel speed, as can be seen in Table 9.

Table 9 - 3DPMD process parameters used in fabrication of a wall (120 x 40 x 15) [57]

Layer Number	Current [A]	Travel Speed [mm/min]	Feed Rate [g/min]
1	180	400	29.0
2	160	500	24.5
3-9	150	600	18.0
10-16	150	700	13.5

2.3.2.1 Multi-Material Additive Manufacturing (MMAM)

One of big advantages of 3DPMD is the possibility to continuously blend up to four different powders in the weld pool, combining the advantages of the classical PTA process to multi-material additive manufacturing (MMAM). Using a continuous transition between different material zone, the joint strength can be improved, reducing mechanical and thermal stresses, decreasing the crack propagation potential and the weight [63]. Johnnatan *et al.* [14] showed that a smooth transition has a better performance, when compared to a hard transition, since the chemical composition of structures present a continuous change.

Kevin *et al.* in [72] and [13] showed the feasibility to produce 3-dimensional functionally graded metallic parts, with Ti6Al4V + different contents of WC and austenitic stainless steel and nickel-based alloys, respectively.

Kevin *et al.* [63] also studied the multi-material parts production, with a continuous transition from the super duplex steel 1.4410 to the austenitic steel 1.4404. The

mechanical properties obtain are present in Table 10 , and prove that 3DPMD is suitable to produce functionally graded multi-metal powders components (Table 10).

Table 10 - Mechanical properties obtain from a 3DPMD process with continuous material transition [63]

Sample Labeling	YS [MPa]	UTS [MPa]	F_{Max} [N]	Elong. [%]
A- 100% 1.4410 (Horizontal)	533 ± 0	875 ± 26.2	5095 ± 275.8	23.9 ± 2.9
B- 50% 1.4410 + 50% 1.4404 (Horizontal)	368 ± 4.2	648 ± 21.9	3808 ± 328.5	56.9 ± 2.5
C- 50% 1.4404 + 50% 1.4404 (45°)	413 ± 0.7	669 ± 18.4	2528 ± 74.2	42.7 ± 0.9
D- 50% 1.4410 + 50% 1.4404 (Vertical)	332 ± 12.3	560 ± 25.0	2231 ± 57.5	25.4 ± 5.0
E – 100% 1.4404 (Horizontal)	244 ± 11.3	460 ± 12.6	2715 ± 205.7	47.4 ± 3.7

Khaled *et al.* [69] studied the mixing of several powders in an arc, in order to adapt the local properties to the defined service loads. Then produced a tool to use as application component, who's susceptible to complex thermomechanical loads/stress (Figure 18).

Figure 18 - Final result of a component produced by 3DPMD[69]

The production of complex component geometries with predefined thermomechanical properties, using 3DPMD, based on a virtual CAD component model, by mixing several

powders, allowed to adapt locally the properties to the defined service loads, with crack-free. In this study they also, successfully created a thermo-mechanical simulation model, and demonstrated that using a preheating, the deformation/residual stress on deposited parts was minimized.

2.3.2.2 Studies using different metallic powders

Titanium alloys are the most used in aerospace applications (approximately 80%) and the remaining 20% are mostly used by the chemical industry due to its protective film, which is chemical inert [73], [74].

These alloys have exceptional corrosion resistance (superior to stainless steels), excellent biocompatibility, low density, high specific strength, and a high melting point (1678°C) [74]. However, the limited machinability of titanium, make it very interesting for AM process. The beam-based powder bed process, such as SLM or EBM, currently dominate this market, producing small dimensions components. Although, this type of AM processes have some disadvantages: the limited construction volume and the low build-up rate per time unit. Larger components can be manufactured by different DED processes. 3DPMD is a poorly investigated process and it can be a viable solution, due to its additional advantages.

Kevin *et al.* [15] showed that 3DPMD can be an alternative to the widely used powder bed processes, to produce titanium components, using non-standardized powder. They concluded that compared to standard metal powders for PTA such as austenitic steel 1.4301 with powder particles dimensions of 50 – 150 μm, the heat input necessary was 60% higher to achieve homogenous structures. This results from the higher melting temperature of titanium, and the larger particles diameters. They also observed a similar hardness value between layers (Figure 19), which means, that the different layers cooling rate and the reheating phenomenon, didn't significantly affect the process. The setup used is represented in Figure 15.

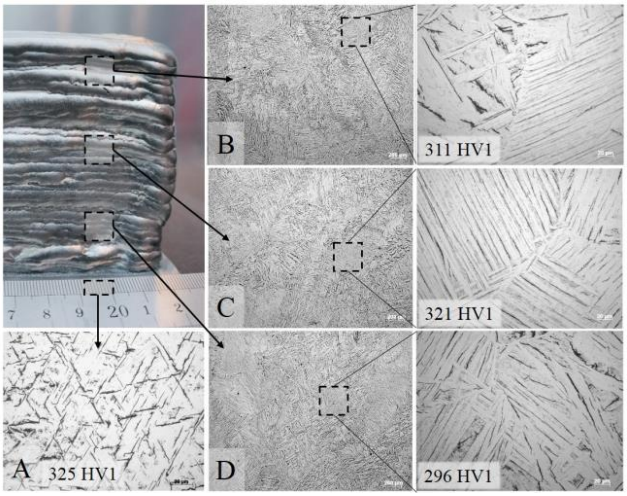

Figure 19 - Comparison of microstructures (A: base material plate; B to D: layer structure) [15]

In other study Kevin *et al.* [62] manufactured titanium parts with 3DPMD and characterized the mechanical properties, testing different loading direction and the effect of post-production heat-treatments. They conclude that the loading direction and the heat-treatment have influence in mechanical properties. The results are presented in Figure 20 and Table 11.

a) **b)**

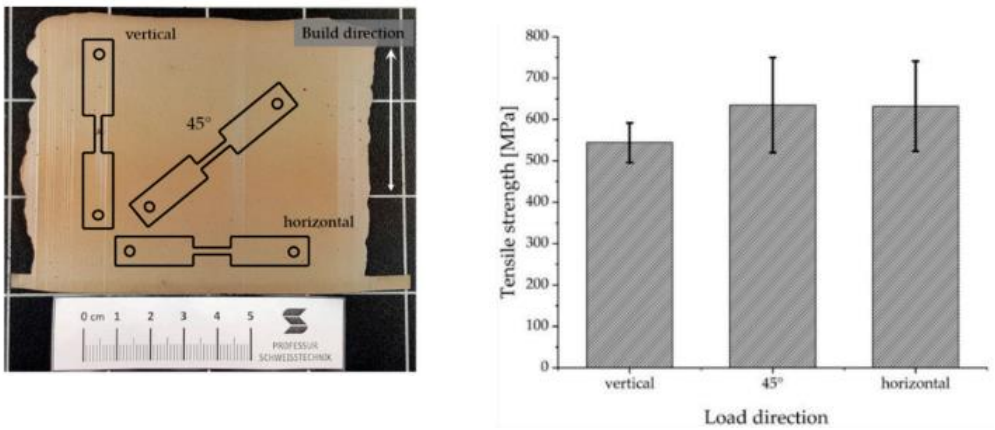

Figure 20 - Influence of the loading direction on the tensile strength: a) schematic of the tensile test specimen orientation, b) results of the tensile tests [62]

Table 11 - Results of the tensile tests for different manufacture conditions [62]

Sample Labeling	YS [Mpa]	UTS [MPa]	F_{Max} [N]	Elong. [%]
none	714	816	3660	80.0
600°C/8h	805	832	3256	32.5
800°C/8h	710	732	2762	47.5

The **Super Alloys** are very important in different industrial sectors (chemical, petrochemical, aerospace, among others), due to high-performance qualities (oxidation resistance, high temperature strength) [75].

In an investigation using a **nickel-based** powder, Eva et al. [57] studied the influence of atmosphere conditions (air and argon) and heat treatments, realizing that, the atmosphere, and the heat treatments, used in this case, had a low impact (Table 12). They also showed viability of the 3DPMD using this powder, since closer standard values were obtained.

Table 12 - Mechanical properties obtained from a 3DPMD process using nickel-based powder [57]

Specimen	Treatment	E [GPa]	YS [MPa]	UTS [MPa]	Elong. [%]
Specimens produced in air atmosphere condition					
1	As Built	197.49	332.32	593.02	16.65
2	TT1	147.00	291.50	660.22	10.94
3	TT2	200.76	303.46	644.32	9.17
Specimens produced in argon atmosphere condition					
1	As Built	144.94	338.14	550.33	15.74
2	TT1	139.18	354.95	661.29	10.86
3	TT2	149.95	350.56	619.69	8.13

TT1: 1120 °C for 20 min (high vacuum furnace under argon atmosphere), cooling by rapid air cooling.
TT2: 1120 °C for 20 min (high vacuum furnace under argon atmosphere), water quenching.

2.3.3 Cold Metal Transfer (CMT)

Originally invented for joining steel to aluminum the Cold Metal Transfer (**CMT)** is a modified method of MIG/MAG process that uses the same principle of 3DPMD, a combination of a robotic movement with a welding torch, however this process uses a welding wire electrode [76].

This is a process that belongs to the Wire Arc Additive Manufacturing (WAAM) based on Gas Metal Welding (GMW). The CMT is a WAAM improved process, that uses a wire electrode that's mechanically moved forward and backward at a high frequency by a secondary wire feeder (Figure 21), allowing to reduce the arc burning time, reducing the energy transfer to the metal [77], [78].

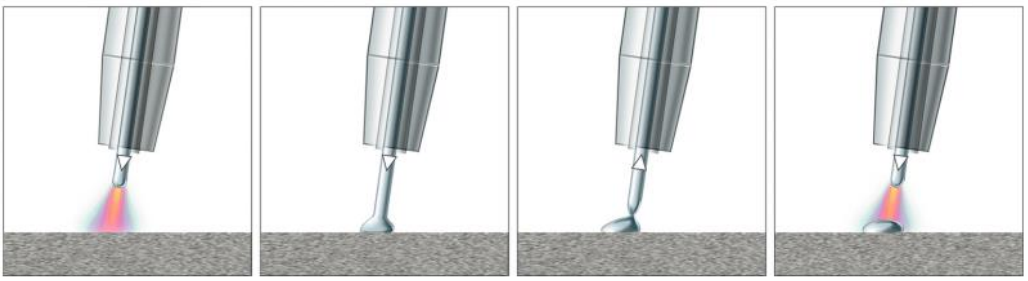

Figure 21 - CMT deposition process representation [79]

The advantages of this process [76], [80], [81] are:

- Possibility to be combine with almost any available robot system;
- Low heat input;
- Possibility to stable manufacture thinner parts, due the low energy input;
- Low spatter;
- High deposition rate.

The disadvantages of this process [79]:

- Only produces lower wall thicknesses;
- High sidewall surface roughness.

2.3.4 Arc-based process control

In general, the DED processes have problems related to the type of solidification. The knowledge of this condition is crucial to be able to define optimized deposition paths and respective machine parameters. In DED process based in arc welding technologies, the weld pool solidification time can be estimated according to welding plates empirical equations present in [71]. According to Equation 5, the solidification time, t [s]:

$$\boldsymbol{t = \frac{LE}{2\pi kpc_p(T_m - T_0)^2}} \quad (5)$$

Where E is the Heat input [J/mm] (from equation 2), L is the heat of fusion [J/g], k is the thermal conductivity [$Wm^{-1}K^{-1}$], p is the density, c_p is the specific heat [$Jmol^{-1}K^{-1}$], T_m is the melting temperature of the material, and T_o is the initial deposition base temperature.

2.3.5 3DPMD vs CMT

Kevin et al. studied the comparison between the wire-based Cold Metal Transfer (CMT), and the 3D Plasma Metal Deposition (3DPMD) [82]. When compared to CMT the advantages of 3DPMD:

- More homogeneous shape of the component produced;
- The heat input and the degree of dilution of the CMT are higher;
- The process is faster;
- The possibility of using different powders, during the welding process.

However, the disadvantage of 3DPMD is the lower degree of material utilization. The results of the study also demonstrated that there is no difference in hardness measurements between CMT and 3DPMD.

In Figure 22 is represented the visual comparison between the same component produced via 3DPMD and CMT, the first process leads to lower distortions and best surface finish.

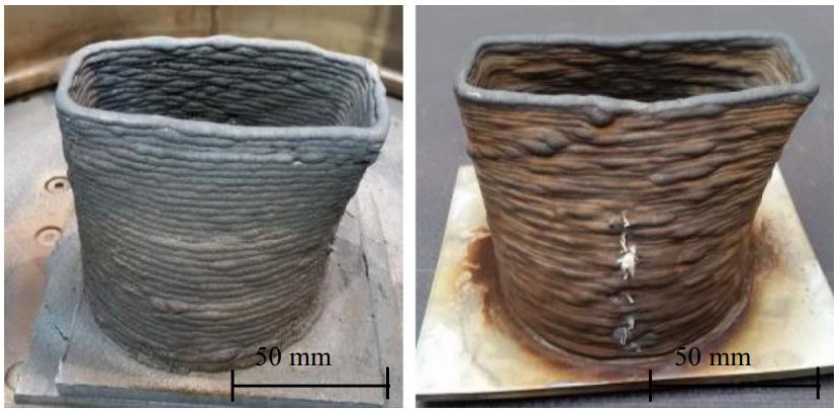

Figure 22 - Generated part (left: 3DPMD; right: CMT) [82]

DEVELOPMENT

3 Development

3.1 Experimental Setup

The 3DPMD process uses a robot with a torch coupled, as mentioned above. For this experimental setup, due the simplicity of the parts to be produced, weld beads, the experimental setup used was a CNC machine with a welding torch couple, for which, was developed G-Code according to the pretended geometries. In Figure 23 – a is represented the setup, the dark tube connected to the torch conduct the protection gas, plasma gas and cooling liquid and the blue tube the powder, attached to the deposition base is the ground clamp.

a) **b)**

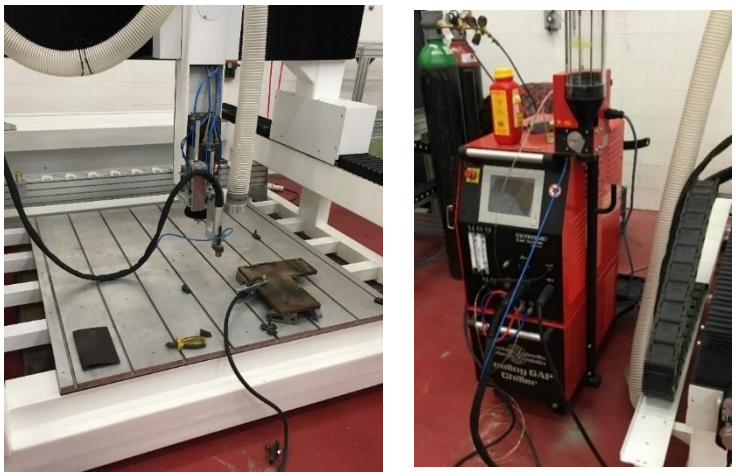

Figure 23 - a) Experimental Setup Used b) PTA machine Setup

In Figure 23 – b is represented the power source, *Eutronic GAP 3511 DC Synergic,* with accessories attached. This welding machine, able to perform Plasma, tungsten inert gas (TIG) and manual metal arc (MMA) welding, has been designed for integrations in automated process or manual operations. In appendix 1 are the specifications of this machine. The control of the PTA machine was manual using a remote control, the *RC-H manual remote control*. *The Cooling GAP – Chiller* was the accessory used to cool the liquid (water), which in turn cools the PTA torch. The accessory used to transfer the powder into the anode nozzle was the *Powder Feeder EP2*. This peripheral has a powder reservoir with 2L capacity, uses Ar or Ar-H2 as carrier gas and the powder feed rate range

varies between 3 and 120 g/min. The value of powder feed rate is related to wheel configuration, torch, anode, and powder density.

Kevin [83] studied the influence of anode nozzle type, in his work he used 3 different types of anode nozzle (4 holes with 2.0mm diameter, 4 holes with 1.2mm diameter and 2 holes with 2.4mm diameter) showing that the anode nozzle type didn't have a significant influence in the geometry. Given the low influence of this parameter, it was chosen to use the anode with 2 holes. The anode nozzle and the torch used are represented in Figure 24 – a) and b), respectively.

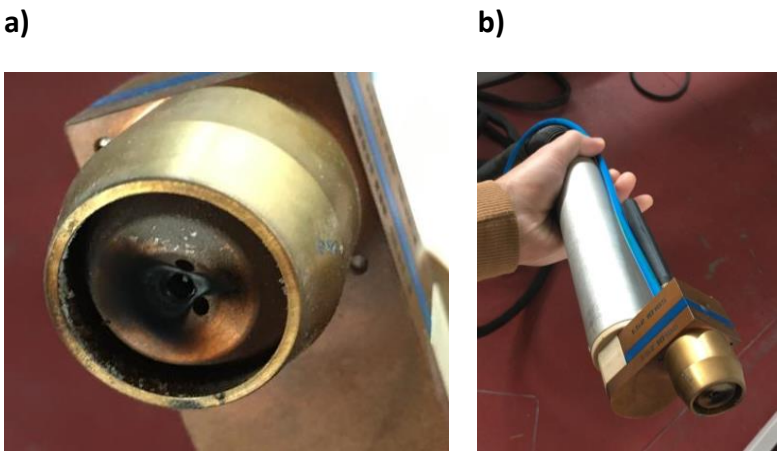

Figure 24 - a) Anode nozzle d_p = 2.4 mm b) GAP E52

The powder feed rate is applied only to a particular configuration as indicated above. Once the setup is defined, the exact powder feed rate was determined. For this purpose, was defined three different percentage settings and the mass determined for a period of 60 seconds. To get valid results, three depositions for each percentage setting were made, and calculated the arithmetic average. Thereafter, linear trend line (Figure 25) was traced from the points registered. The equation 6 is derived from that line, relating the percentage setting and the powder feed-rate.

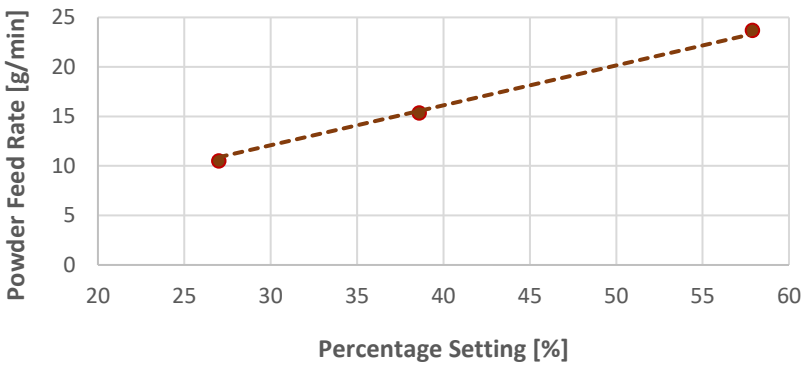

Figure 25 - Relation between Percentage Setting and Feed Rate

$$\boldsymbol{Feed\ Rate} = \mathbf{0,403} * \boldsymbol{Percentage\ Setting} \quad (6)$$

In appendices 6.1 to 6.4 are presented the technical characteristics of the peripherals mentioned above.

The base platform employed for the depositions was 30 millimetres height carbon steel board (the chemical composition is represented in Table 13). This material present has a hardness of 170 to 210HV. Before the depositions the surface of this material was cleaned by brushing.

Table 13 - Chemical Composition of base platform (appendix 6.6)

Element	C	Mn	Si	P	S	Fe
Concentration (%)	0.412	0.679	0.240	0.010	0.003	Bal.

3.2 Design of Experiments

Additive Manufacturing processes are characterized by a layer built-up, being crucial the stability of the process, consequently, the exact knowledge of the relations between the process parameters and the component geometry produced is determinant to the success of this type manufacturing.

The Design of experiments (DoE) specifications were followed, to analyze the process. DoE is a systematic method that allows to reach valid and objective conclusions from an experiment. DoE includes planning, designing, conducting, and analyzing, to determine the influence and the relationship between factors on the outputs of the process. The knowledge and integration of statistical tools in the design methodology is the key to efficient and successful results [84].

In Figure 26 are represented the setting parameters of 3DPMD Process. The Gas Parameters are the respective amount and type of shielding gas, plasma gas and conveying gas. The Process Parameters are welding speed, welding current, electrode set back, electrode angle and powder feed rate. The raw material comprises the particle size, chemical composition, and number of different materials combined.

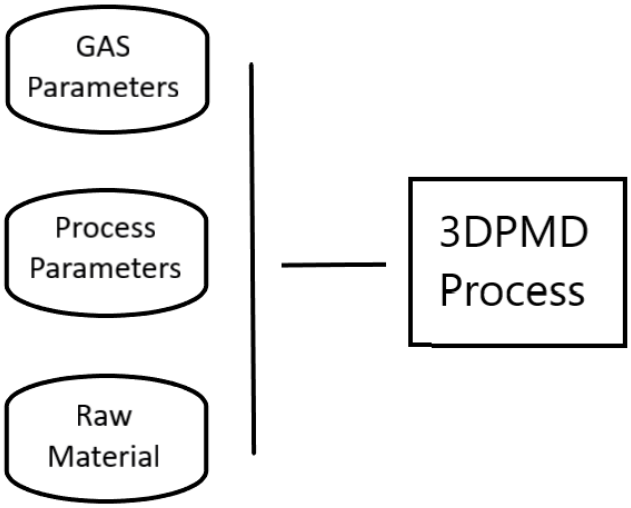

Figure 26 - Setting Parameters of 3DPMD Process

After the preparation of machine setup, the planning of experiment was taken, starting with choice of factors and response variables. Following that, the designing phase starts with the selection of number of levels and the respective ranges. Finally, the depositions were performed and the subsequently processing of the results.

3.2.1 Full Factorial

In this work was used a Full Factorial Experiment (FFE). A FFE consists in the study of all possible combinations of the factors (process parameters) and the levels. The total number of experiments to run is given by L^k, where L is the number of levels and k the total number of factors [85].

3.2.2 Selection of Control Factors and Responses

The main objective of this work is to find the influence of process parameters on the geometry (wall thickness and layer thickness), and microhardness. The most relevant parameters for the 3DPMD process were chosen based on the literature found, being the welding current, welding speed and powder feed rate. Consequently, the aim of this study is to prioritize the effect of this process parameters through the run of various experiments. These parameters were the control factors since they directly influence the properties of the produced component.

3.2.3 Fixed Parameters

The process parameters and the gas parameters presented in Table 14 were established according to the consulted literature and were maintained constant for all the depositions.

Table 14 - Process Fixed Parameters

Parameter	Parameter Setting
Electrode Set Back	2.5mm
Electrode Angle	30°
Plasma Gas Amount (Type)	1.5 l/min (Argon)
Shield Gas Flow Rate (Type)	15 l/min (Argon)
Conveying Flow Rate (Type)	1.8 l/min (Air)

The raw material selected was the commercially designated *Eutroloy 16604*. This powder has a spherical shape and a high level of purity with low dissolved oxygen content, being made by gas atomization [86].

This alloy is characterized by excellent heat resistance, thermal shock and corrosion and good resistance to cracking [16]. The chemical composition of this powder is represented in Table 15.

Table 15 - Chemical Composition of Eutroloy 16604 [16], [86]

Element	C	Cr	Co	Mo	Fe
Concentration (%)	0.20	15	15	2.5	Bal.

The main applications for this powder are tools for hot and cold metal shaping, clipping bed, rolling mills, bending machines, sealing joints. In literature found, only Khaled et all. [69] tested this material in 3DPMD process, however mixed with an iron-based alloy. For this purpose and due to the properties of this alloy, in this work the Eutroloy 16604 was isolated investigated.

3.3 Test 1 and Test 2

Since this process is very recent, it was decided to study several possible values for welding current and speed, as well as the possible interactions between them, without putting the powder feed rate in the test matrix. The chosen of the levels values was also based in literature (Table 16), with the objective of verifying or confirming if with this metallic alloy the behavior of the responses would be similar. In the two tests the powder feed rate was kept constant, with a value of 10.4 g/min and 20 g/min, respectively. This results in a 6^2 (36) runs for each test. The depositions tests are represented in Figure 27.

Table 16 - Factors and Levels of FFE for the tests 1 and 2

	Levels					
Factors	1	2	3	4	5	6
Welding Current [A]	70	90	110	130	150	170
Welding Speed [mm/min]	100	200	300	400	500	600

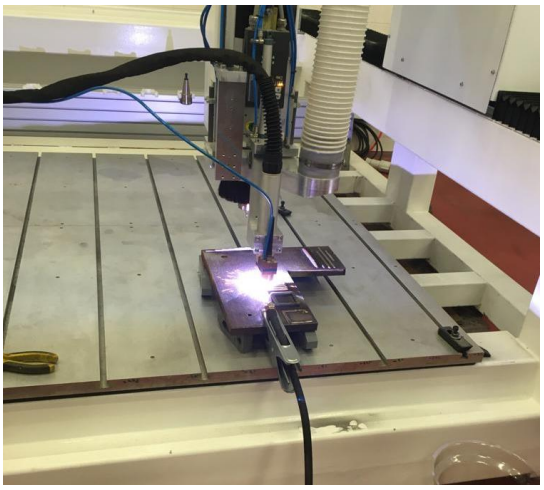

Figure 27 - Representation of the Deposition Process

3.3.1 Preparation of Samples and recording of results

To evaluate the properties of the parts produced, 24 individual specimens were obtained by cutting the deposition plate, according to the microscopy and microhardness tester area. Each specimen contains 3 cross-section weld beads with the same welding current setting.

Several cuts where needed to obtain these specimens. For the cutting process chosen, the maintenance of the parts properties was considered a priority, as such, a non-generation of heat process was required. However, the Electric Band Saw from ISEP didn't have the range to cut the plate where the weld beads were deposited (450x390mm). For this propose, 5 cuts were performed by Abrasive *Water Jet (AWJ) Cutting* in an external enterprise, *StatusAlumínio,* to obtain 4 parts from the original plate. AWJ (Figure 28 – a) is a non-traditional cutting technique that uses high-velocity water containing abrasive particles and can be used for different materials with different thickness, from ductile (aluminum, brass, steel, titanium, and nickel-based alloys) to brittle (glass, ceramics, stone), or even for soft materials (rubber or foam) and composite materials. The main advantages of this process are the lower tool wear (lower cutting forces and higher productivity), cutting precision, high range of materials and high thickness cuts [87]–[89]. Subsequently, the final cuts were performed in ISEP. The longitudinal in the electric band saw (Figure 28 – b), and then the transversal, due to the hardness of the weld beads, it was use an electric disc saw (Figure 28 – c) with a ability to cut high hardness materials.

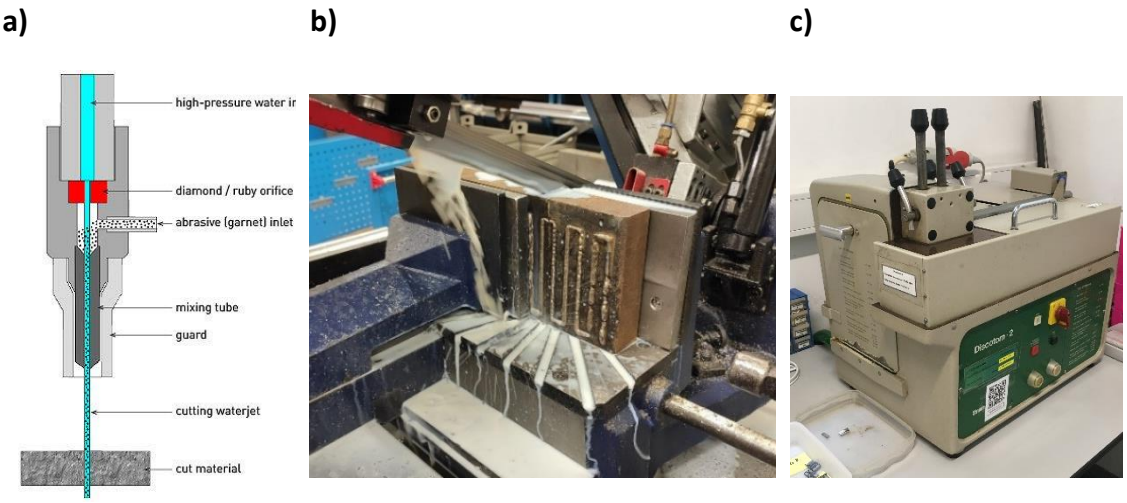

Figure 28 - a) Abrasive Water Jet Cutting Illustration [90] b) Electric band saw cutting c) Discotom 2

Subsequently, the specimens were soaked in epoxy resin using molds, and then, prepared according to the standard metallographic *ASTM E3-11* [91].

First the specimen's surface was grinded, using three different sandpapers with particles of silicon carbide (SiC), of decreasing granulometry (220, 500 and 1000), to eliminate the surface risks. After that, the surfaces were polished to standardize the surface, using two abrasives containing diamond particles starting with 3 µm size and finishing with 1µm.

The final step, that allows to reveal the material structure was the chemical attack. To proceed with this step, it was necessary to find the appropriate reagent, after unsuccessful testing the *Nital* and a reagent used for stainless steels, consulting the bibliography were successfully tested a solution typically used for Inconel alloys, which contain 2g of perchloride Cu, 40ml of hydrochloric acid (HCl) and 60ml of ethyl alcohol. To proceed the attack, a piece of cotton was soaked in this solution and with the help of a tweezer three passages were made in each sample, and immediately washed with running water to eliminate the reagent from the surface, finishing that way the reaction. The accuracy of procedure was firstly tested because there was not a reference attack time for this material.

In Figure 29 is represented the metallographic specimen after the preparation.

Figure 29 - Metallographic Specimen after the preparation

The equipment used to record the sample's microstructure was the microscope *Olympus SZ-PT* with the *Olympus* DP70 camera attached (Figure 30).

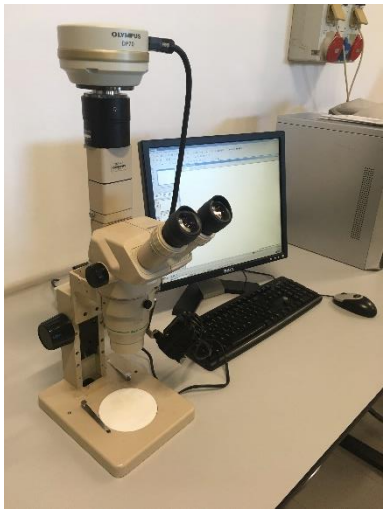

Figure 30 - Microscope Olympus SZ-PT and Olympus DP70 camera

To measure the hardness of the weld beads, given their size and intending to obtain hardness gradients resulting from thermal variations generated in the deposition process, it was decided to perform microhardness measurements. This test is performed by exerting a continuous load on the material for a certain period. The equipment used was the microhardness tester *Duramin* (Figure 31).

Figure 31 - *Duramin* microhardness tester

The measurements were carried out in accordance with the ISO 6507-1 [92], making indentations with a spacing of 1 to 3mm, during 5s. The number of indentations and the spacing between them depended on each deposited bead dimensions and the zone where it was measured, following a line from the top to the base material. The measurement of the Vickers hardness was based in equation 7, where F is the press load (9,807N) and d is the average of the diagonal lines (d1 and d2 - Figure 32).

$$\boldsymbol{Vickers\ Hardness} = \mathbf{0,1891}\frac{\boldsymbol{F}}{\boldsymbol{d^2}} \tag{7}$$

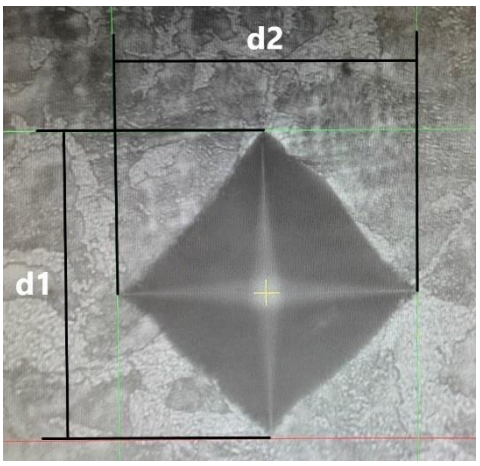

Figure 32 - Indentation diagonals (40x magnification)

3.3.2 Results

In this subchapter are present the results obtained. The statistical data analysis was performed using *Excel* 2019® and *MiniTab* 21.2®. The descriptive analysis consisted in the determination of central tendency and dispersion measurements, average and standard deviation, respectively (appendix 6.5). To evaluate the possible correlations between factors the ANOVA test was applied, however no evidence of interaction between factors was found. In this way, the focus was given to the effect of each factor individually. To study the influence of control factors (welding current, welding speed and powder flow rate) in the geometry and hardness of produced parts, main effect plots together with Spearmen's correlation coefficient were used. The Spearmen's correlation coefficient measures the correlation between variable pairs. It was considered statistically significant, a critical significance level (p) of less than 0.05. The microstructure evolution and the aspect of the weld beads was descriptively analysed and with the help of hardness variation graphs.

3.3.2.1 Welding Current

In Table 17 are represented the values obtained for Spearmen's correlation coefficient (r_s) and the p-value (p) between welding current the geometry and the hardness. The negative signal of this value corresponds to a negative influence correlation.

Table 17 - Correlation between welding Current, the geometry and the hardness

Response	Test	r_s	p
Wall Thickness	1	0.592	<0.001
	2	0.701	<0.001
Layer Thickness	1	-0.567	<0.001
	2	-0.263	0.121
Hardness	1	-0.027	0.878
	2	0.454	0.005

The results show that, the increase of welding current leads to a decrease of layer thickness and an increase of wall thickness. Keeping the other process parameters constant, the welding current increase leads to the increase in the energy input per unit length, E (Equation 2), as well as the melt pool size. The temperatures that the melt pool

reach are higher, consequently the fused metals present lower viscosity, which is not favourable to a perpendicular built-up. In this way the layer thickness decreases with increasing current.

Contrary to what was expected, in test 2 the layer thickness shows a weak correlation. The reason for that is a deviation occurring for a welding current of 90A (Figure 34 - right), that can be related to uncontrol unknown factors.

The average values obtained for the hardness are in small range (540HV to 650HV), which allow to conclude that the hardness does not vary much with the variation of the control factors. In test 2 can be seen a moderated (p=0.005) positive correlation (r_s=0.454), as welding current increases the hardness also increases, however given the results obtained in test 1 (p=0.878, r_s=-0,027), no statistically significant correlation can be assumed. More tests would be needed to conclude their relationship.

These results, and the variations described can also be seen in the main effect plots, present in Figure 33, Figure 34 and Figure 35.

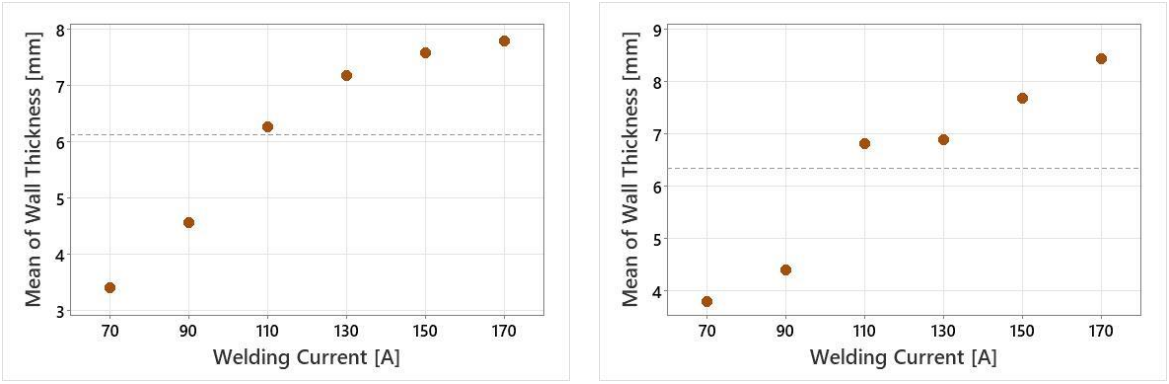

Figure 33 - Main Effects Plot of Welding Current for Wall Thickness: Left -Test 1, Right - Test 2

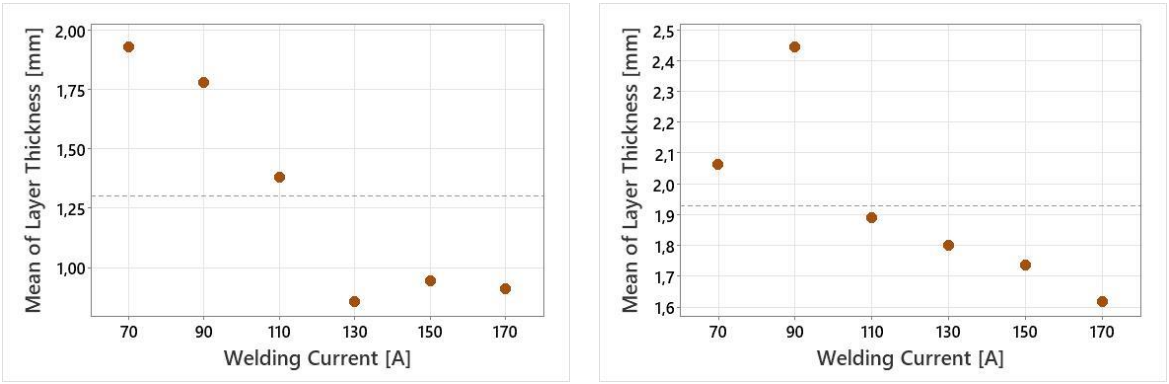

Figure 34 - Main Effects Plot of Welding Current for Layer Thickness: Left -Test 1, Right - Test 2

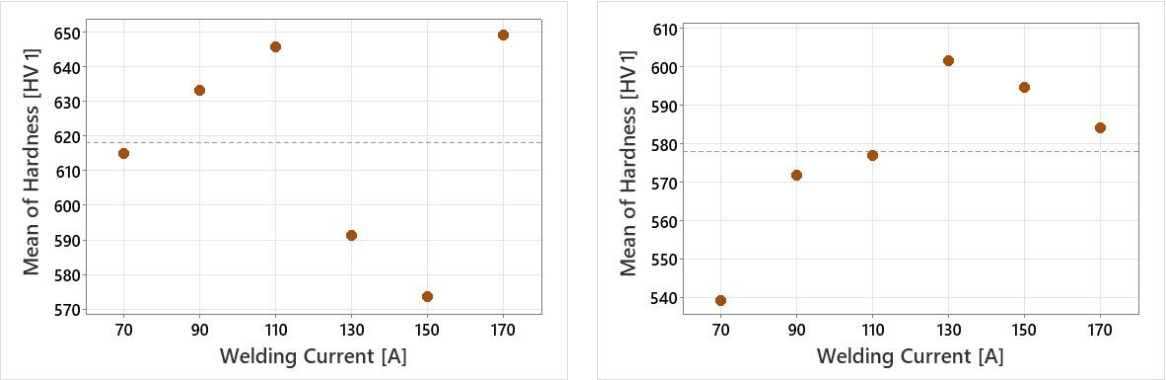

Figure 35- Main Effects Plot of Welding Current for Hardness: Left -Test 1, Right - Test 2

3.3.2.2 Welding Speed

Table 18 presents the values obtained for *Spearmen*'s correlation coefficient and the p-value (p), between welding speed the geometry and the hardness. The increase in the welding speed, causes the wall and layer thickness decrease. In this case, the increase of the welding speed leads to a smaller weld pool size, due to the reduction of interaction time, affecting directly these two parameters. No statistically significant relation between this parameter and the hardness values was found (p=0.281 and 0,663, r_s value of -0,185 and -0,075).

Table 18 - Correlation between Welding Speed, the geometry and the hardness

Response	Test	r_s	p
Wall Thickness	1	-0.695	<0.001
	2	-0.617	<0.001
Layer Thickness	1	-0.705	<0.001
	2	-0.890	<0.001
Hardness	1	-0.175	0.281
	2	-0.075	0.663

In the main effect plots, present in Figure 36, Figure 37 and Figure 38 is possibly to seen these correlations and the respective mean values ranges.

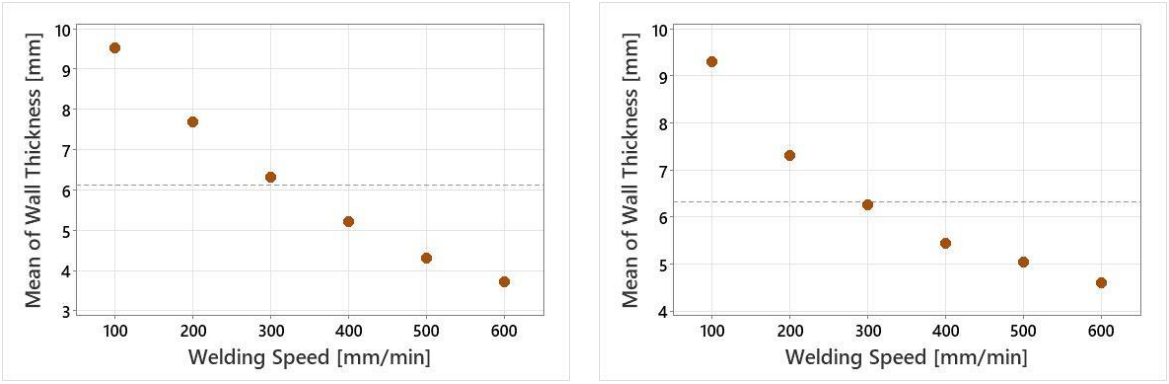

Figure 36 - Main Effects Plot of Welding Speed for Wall Thickness: Left -Test 1, Right - Test 2

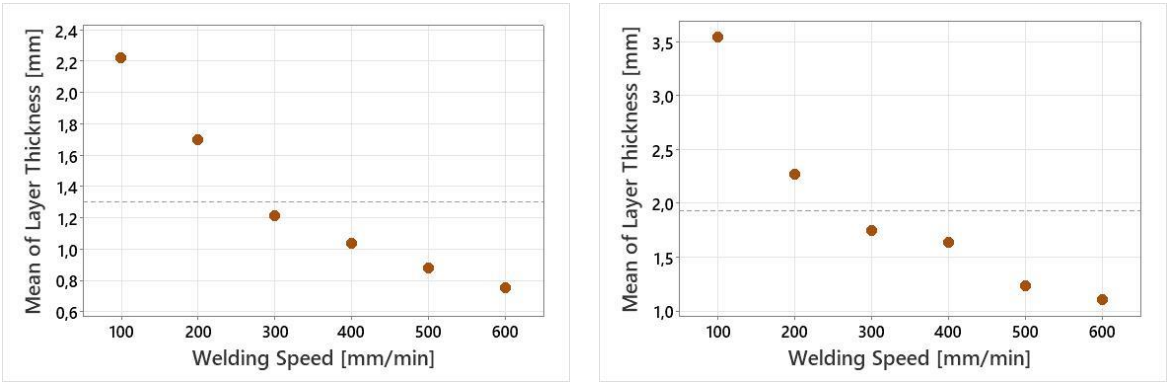

Figure 37 - Main Effects Plot of Welding Speed for Layer Thickness: Left -Test 1, Right - Test 2

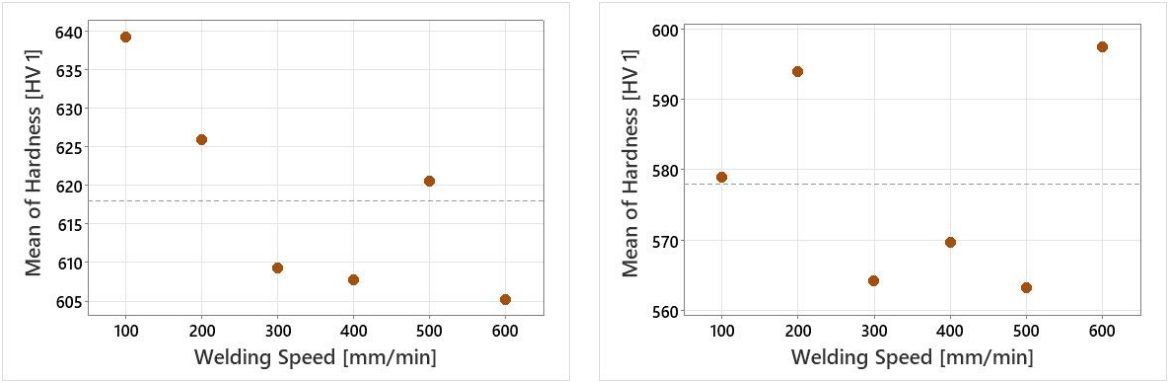

Figure 38 - Main Effects Plot of Welding Speed for Hardness: Left -Test 1, Right - Test 2

3.3.2.3 Powder Feed Rate

To evaluate the influence of powder feed rate in the geometry and hardness, the results of tests 1 and 2 were combined. As mentioned above, the study of the influence of welding current and speed was a priority. Despite the need to perform more tests, using more levels for the powder feed rate, the results obtained allow us to visualise the influence of this control factor. In Table 19 are present the values obtained for *Spearmen*'s correlation coefficient and the p-value (p) between powder feed rate and the different responses.

Table 19 - Correlation between Powder Feed Rate and wall thickness, layer thickness and hardness

Response	r_s	p
Wall Thickness	0.074	0.539
Layer Thickness	0.398	0.001
Hardness	-0.434	0.000

The results show, the increase in powder feed rate resulted in a higher layer thickness (positive correlation, r_s=0.398 and p=0.001). The wall thickness variation is not significant (r_s=0,074 and p=0,539). This can be explained by using the equation of the required amount of heat, Q_i (equation 3 and equation 4). Setting the same energy input, increasing the mass input of filler material per unit length, the temperature on melt pool tends to decrease. The heat capacity, c_i, the welding time, t_s, and the initial temperature can be neglected due to material constancy or equal construction assuming time. In this way can be conclude that using a powder feed rate of 20g/min the temperature is 50% lower, compared with a powder feed rate of 10.4g/min (deduction in equations 8 to 11).

$$\boldsymbol{m_1 \cdot T_1 = m_2 \cdot T_2} \tag{8}$$

$$\frac{\boldsymbol{m_1}}{\boldsymbol{m_2}} = \frac{\boldsymbol{T_2}}{\boldsymbol{T_1}} \tag{9}$$

$$\frac{\boldsymbol{10,4}}{\boldsymbol{20}} = \frac{\boldsymbol{T_2}}{\boldsymbol{T_1}} \tag{10}$$

$$\boldsymbol{T_2 = 0.52 \cdot T_1} \tag{11}$$

Lower temperatures lead to higher material viscosity, being favourable to a perpendicular built-up, consequently the layer thickness increase.

In relation to hardness, a negative correlation was observed. However, the range of hardness values obtained is very small, concluding that this variation is not very significant, approximately 580 to 620 HV.

In the following main effects plots (Figure 39) are represented the influence of powder feed rate in layer thickness, wall thickness and hardness when compared to welding speed and welding current. It can also be seen that the powder feed rate has practically no influence on the wall thickness, as found through the values in the Table 19.

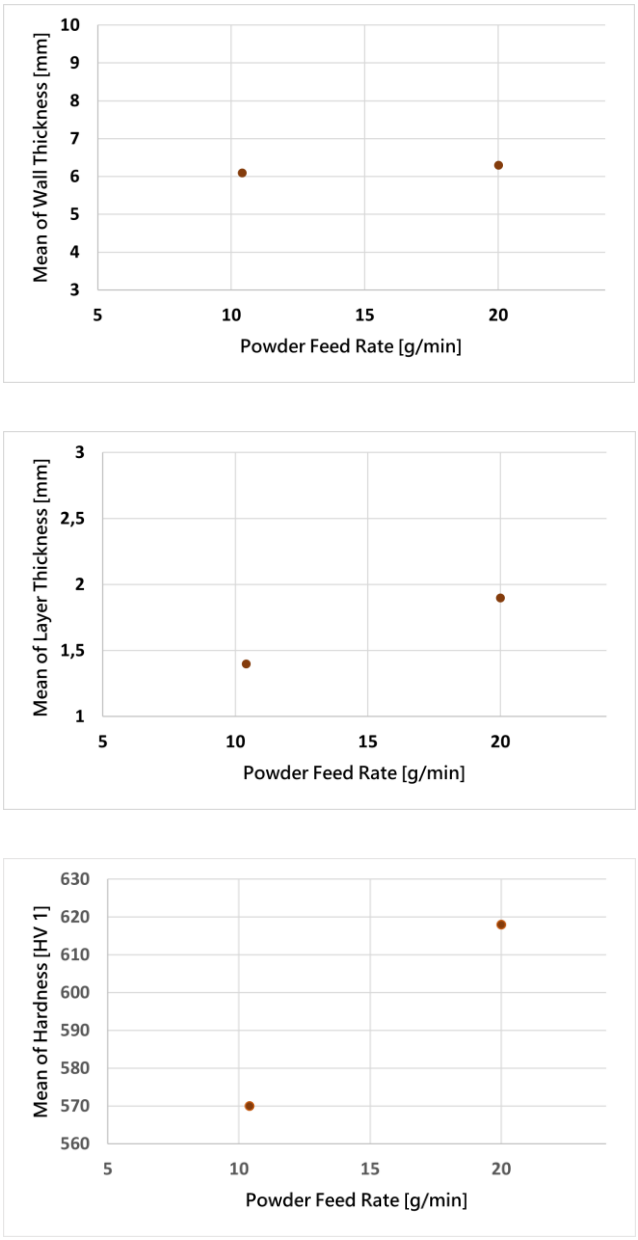

Figure 39 - Main Effects Plot of the powder feed rate on three responses

3.3.2.4 Quality of weld beads

The study of weld beads quality as a whole, and the effects of factors on final quality, is as important as the study of the influence of each factor in each response. Besides the height, H, and width, W, (layer and wall thickness) of the weld beads, the aspect, the dilution (D), presented in Equation 12, the wetting angle (θ), the aspect ratio (given by the ratio between measured width and height of the weld bead), and consequently the heat affected zone must be considered [93]. In Figure 40 are represented some of these parameters. The wetting angle, the dilution percentage and the aspect ratio are related, and their values, give relevant information about a regular deposition and a good adhesion between deposited beads and base material.

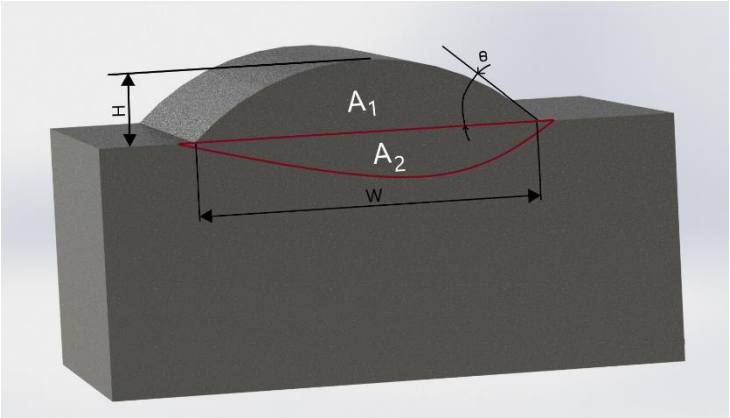

Figure 40 - Transverse cross-section of a weld bead

$$\boldsymbol{D = \frac{A_2}{A_1 + A_2} \times 100\ [\%]} \tag{12}$$

The aspect ratio and wetting angle are related, and consequently their influence to quantify the weld beads quality. The wetting angle should not be too high, as this reduces adherence. In extreme cases it can result in a spherical shape, which also conduces to the formation of porosity between layers when constructing a multilayer geometry. The range of values for the wetting angle and the aspect ratio depends on the process used, for the 3DPMD process there wasn't found a reference value.

The dilution percentage is also very relevant to achieve a strong fusion bond between the weld bead and the base material, however, this value must be small as possible, reaching a small depth of melt, in order to obtain pure layer (not diluted by the base material), and in order to reduce the heat affected zone (HAZ) [94].

Figure 41 shows that, the weld beads obtained for a welding current of 70A and 90A, a welding speed from 100 to 600mm/min, and a powder feed rate of 10.4g/min and

20g/min. 10.4g/min powder feed rate setting, results in an irregular deposition for all weld beads. Using 20g/min powder feed rate can produce regular depositions for lowest welding speed. This happens because a high volume of material is fed into a low energy melt pool (low welding current), leading to partial melting, and stacking of filler material. In all the weld beads produced the wetting angle tends to be high.

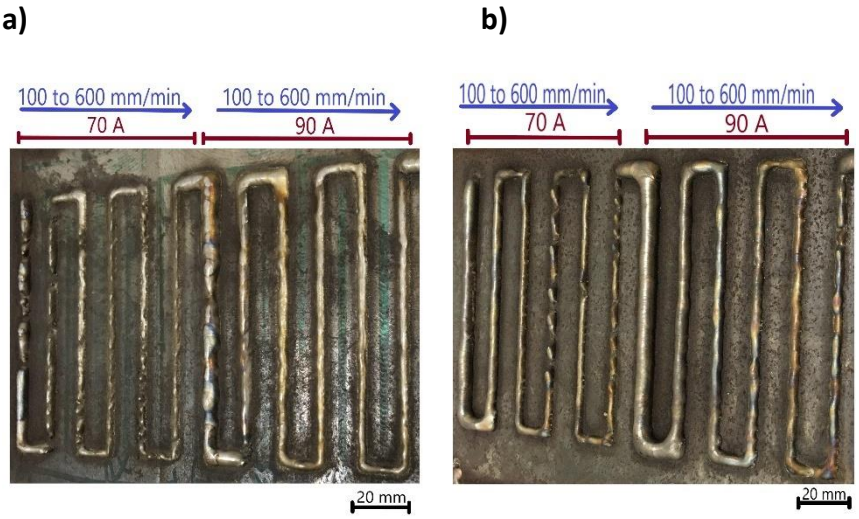

Figure 41 - Comparison between different powder feed rate, a) 10,4 g/min, b) 20 g/min

Figure 42 shows the weld beads obtained for a welding current of 110A and 130A, a welding speed from 100 to 600mm/min, and a powder feed rate of 10.4g/min and 20g/min. The weld beads present a regular deposition for the lower powder feed rate, however for the highest powder feed rate the depositions aren't total regular, principally at lowest welding speeds.

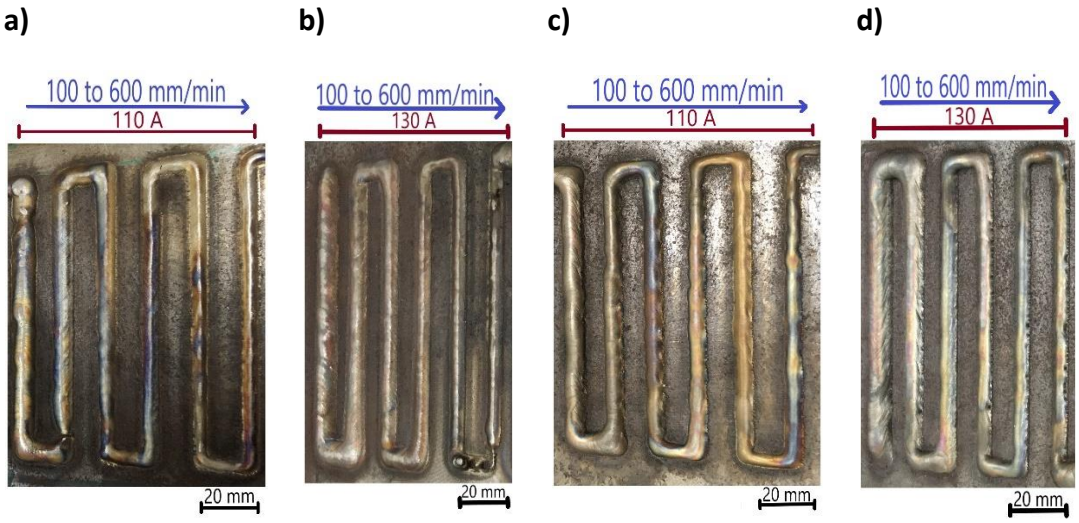

Figure 42 - Comparison between different powder feed rate, a) and b)10,4 g/min, c) and d) 20 g/min

Figure 43 shows the weld beads obtained for the max welding current used in the two tests performed (150A and 170A). Higher current also represents higher energy delivered to the melting pool.

For 10.4g/min powder feed rate setting, the weld beads present very low quality. The weld beads produced at the lowest welding speed present a phenomenon call dripping. The reason for that occurrence is the very high plasma power density available for high interaction times and low feed rates, leading to melting and evaporation of the deposited material. This non-uniform deposition is also described by Jhavar *et all.* [95]. The described combination also contributes to the appearance of cavities, resulting from excessive melting of the base material. In Figure 44 is represented the cross-section of weld beads produced under these conditions, where the cavities are visible, with the largest being about 2mm wide. For 20 g/min powder feed rate setting the weld beads present a good quality with a regular deposition.

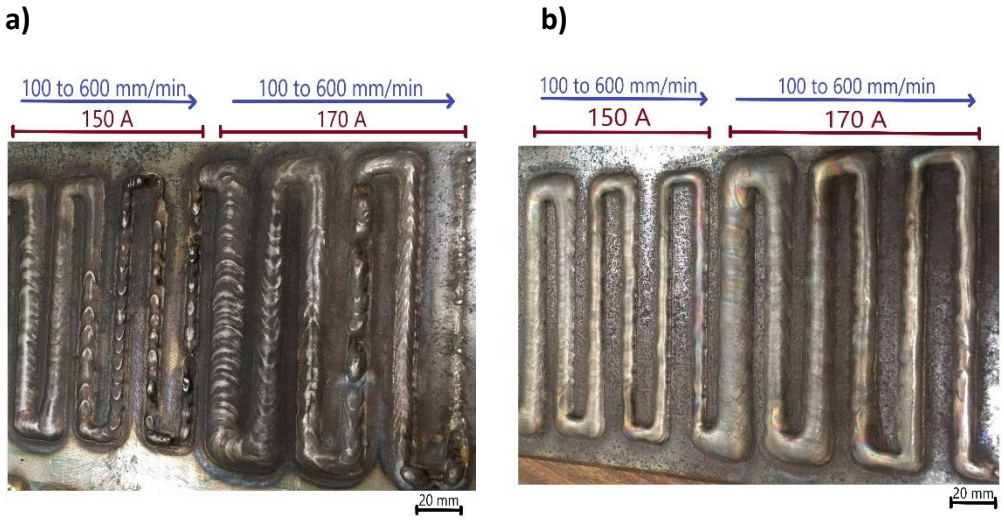

Figure 43 - Comparison between different powder feed rate, a) 10,4 g/min, b) 20 g/min

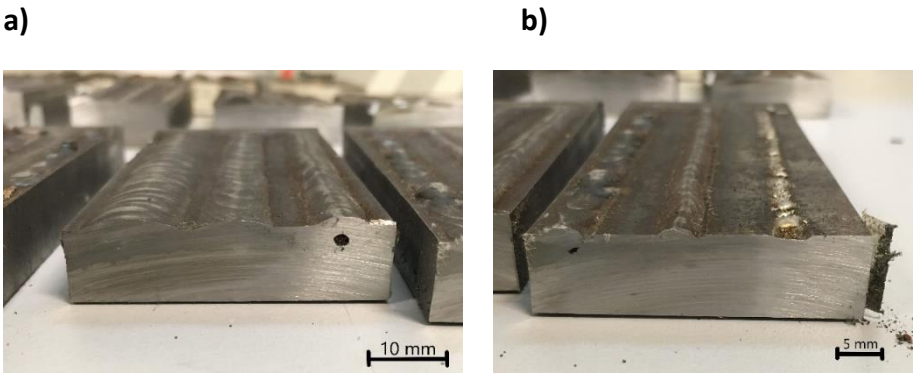

Figure 44 - Cross-section of weld beads with 10.4g/min powder feed rate and a welding current of: a) 100 to 300mm/min, b) 400 to 600mm/min

From the results can be concluded that, combining high welding current with lower powder feed rates, leads to an irregular deposition with formation of cavities, which allows to conclude that higher welding current requires higher powder feed rate.

The welding speed also have influence in the quality of weld beads helping to improve the conditions, however, the welding speed must not be too high, principally when using low welding currents.

The best combination of welding current, welding speed and powder feed rate also depends on the desired geometry. By visual inspection, the most acceptable weld beads (better geometric and surface quality) were obtained using a powder feed rate of 20g/min combined with a welding current of 70A, 90A, 110A, 130A (using low welding speed, 100 and 200 mm/min) and 150A, 170A. Using a powder feed rate of 10,4g/min only combined with a welding current of 110A and 130A.

3.3.2.5 Hardness and Microstructure Evolution

According to the specifications of the powder used, the hardness of the material, excluding the dilution zone, is approximately 45HRC, which corresponds to 450HV. The hardness values obtained for all the weld beads were higher (between 500 to 700HV).

Due to the similarity of the hardness variation curves and the respective microscopic images obtained between deposited beads, to present their hardness behavior and the respective microstructure, seven were selected. For the calculation of the approximate dilution percentage based on a geometrical approach, a python script was developed, using the *OpenCv* library. *OpenCv* is a python open-source library, Cv is an abbreviation form of a computer vision. This library is used for computer vision in artificial intelligence, machine learning, face recognition, among others [96]. This library was used to read the weld beads microscopic images, process them, and identify their contours, to calculate their areas and thus obtain the approximate calculation of the dilution percentage. The *Matplotlib* library was used to visually present the results obtained. "*Matplotlib* is a comprehensive library for creating static, animated, and interactive visualizations in Python"[97]. In appendix 6.9 is represented the written code in IDE *Jupyter Notebook*, with respective annotations and results for the calculation of approximate dilution percentage of weld bead 1.

In the graphs of the Figure 45 to Figure 51, it is possible to identify the three different hardness zones, the weld bead, the HAZ and the base material. In the respective microscopic captures, it is possible to see just the first two of these three zones.

The HAZ near the weld bead has more refined grain structure and a hardness value similar to the deposited bead. However, this area is very small, and quickly transits to a coarser grain size area, visible in the images, presenting harness values between 300 and 500HV. Finally, not visible in the images, the base material present hardness values between 170 and 210HV.

The three zones considered in the figures (Weld Bead, HAZ and Base Material) were considered taking into account the typical hardness of the deposited material and the base material.

The results of hardness variation in the weld beads are in line with the results presented and discussed previously, as well as the elations to be withdrawn.

The weld bead of Figure 45 had a higher dilution percentage compared to the weld bead of Figure 46, a result of the longer interaction time with the base material during deposition.

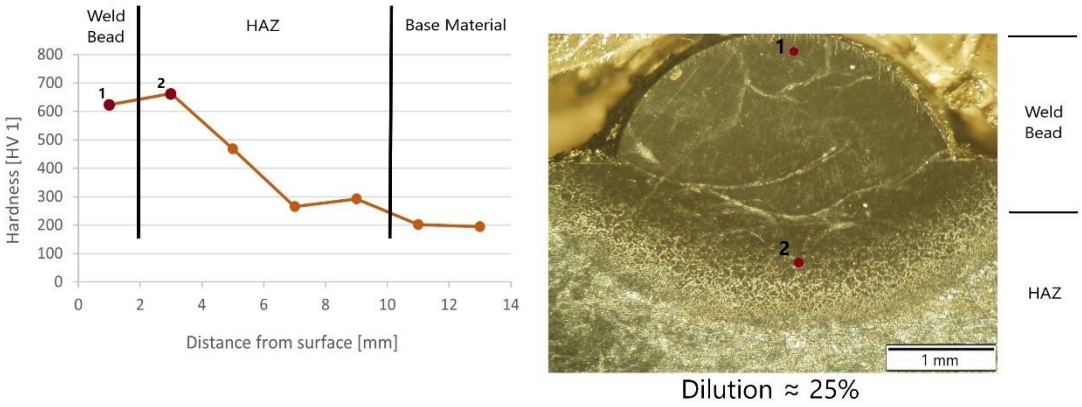

Figure 45 - Welding Current: 70A; Welding Speed: 100mm/min; Powder Feed Rate: 10.4g/min (1)

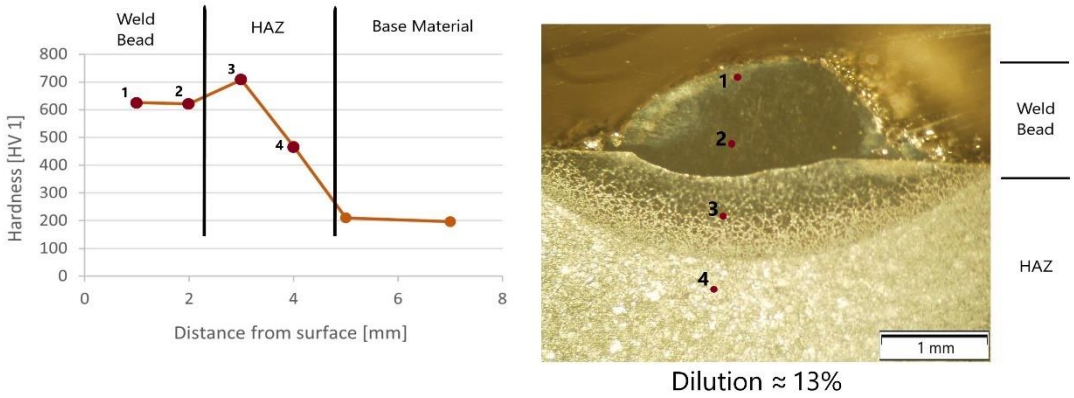

Figure 46 - Welding Current: 70A; Welding Speed: 600mm/min; Powder Feed Rate: 10.4g/min (6)

The weld bead of Figure 47, produced with a high welding current (170A), a low powder feed rate (10.4g/min), and a medium speed (300mm/min), had a high penetration in the base material, as well as, the dilution percentage, approximately 38%.

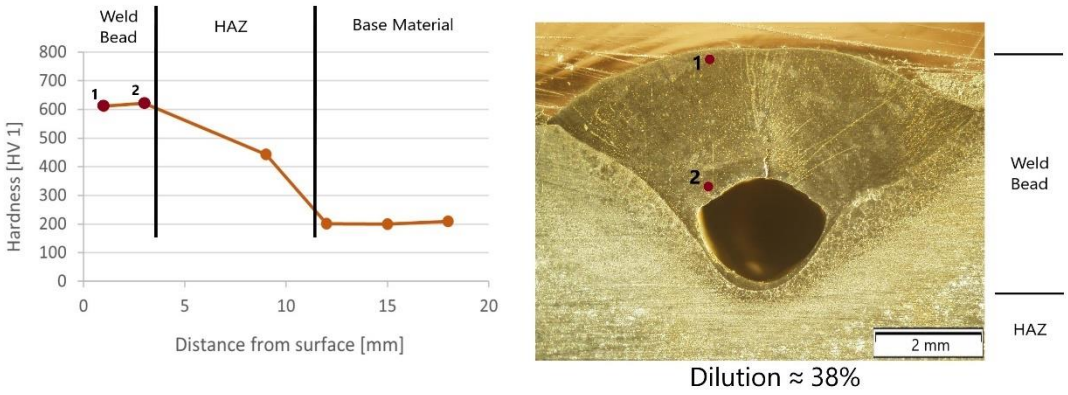

Figure 47 -Welding Current: 170A; Welding Speed: 300mm/min; Powder Feed Rate: 10.4g/min (33)

The deposited beads of Figure 48 and Figure 49, produced with a welding current of 110A and a welding speed of 200 and 400mm/min, present a dilution percentage of 16 and 21%, respectively.

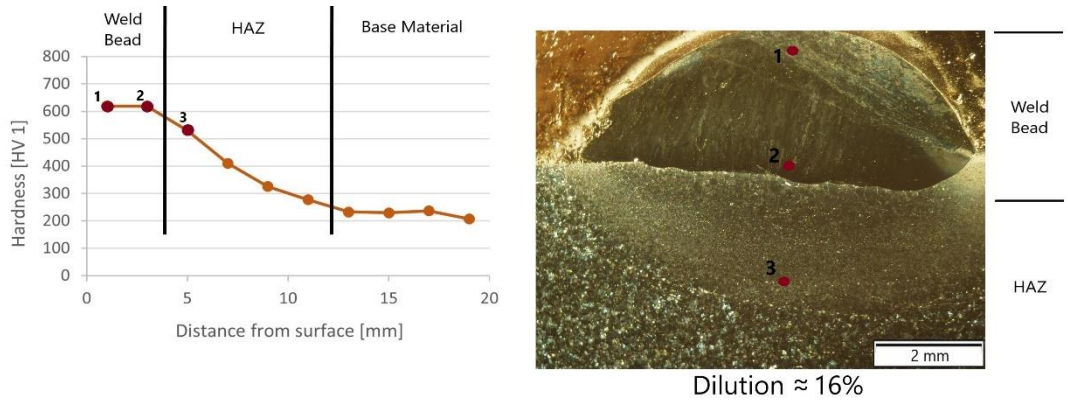

Figure 48 - Welding Current: 110A; Welding Speed: 200mm/min; Powder Feed Rate: 20g/min (50)

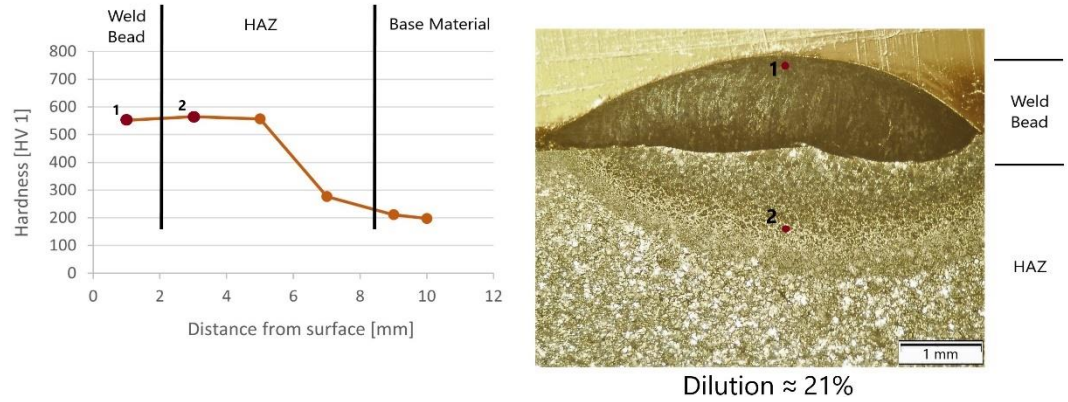

Figure 49 - Welding Current: 110A; Welding Speed: 400mm/min; Powder Feed Rate: 20g/min (52)

The weld beads of Figure 50 and Figure 51, with a high welding current (130A) and a welding speed of 400 and 500mm/min, present high dilution percentage, 27 and 33%, respectively.

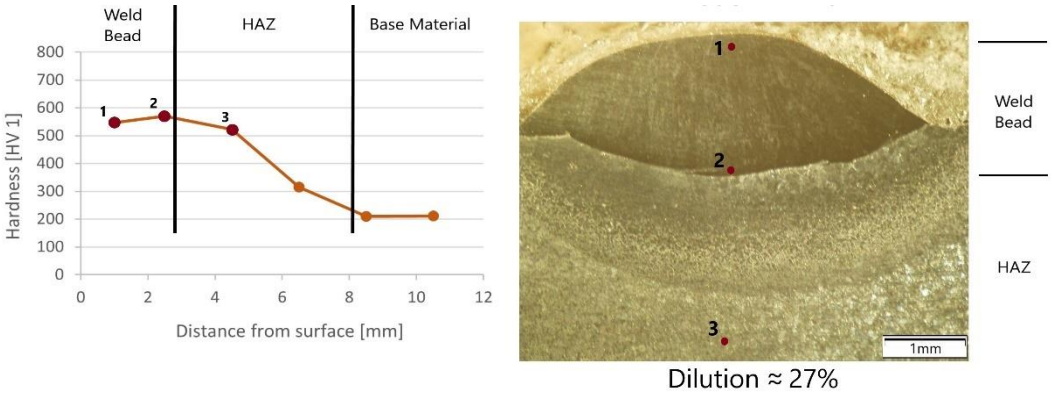

Figure 50 - Welding Current: 130A; Welding Speed: 400mm/min; Powder Feed Rate: 20g/min (58)

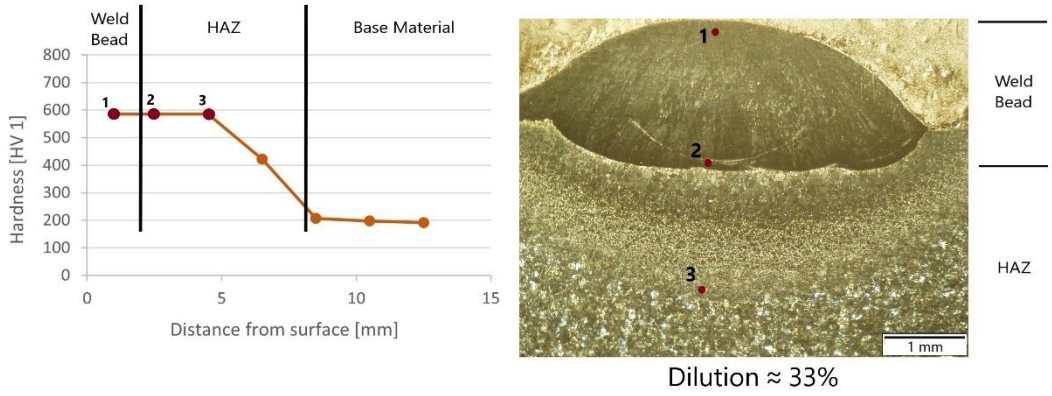

Figure 51 - Welding Current: 130A; Welding Speed: 500mm/min; Powder Feed Rate: 20g/min (59)

3.4 Geometry Production

After performing the Tests 1 and 2, with the aim of testing the production of a geometry and what would be the evolution of hardness in overlapping layers, a cube geometry has been produced. It was decided to produce a fully filled cube with a dimension of approximately 50x50mm. To this end, considering the results obtained (Table 20), has been defined: welding current: 90A, welding speed: 200mm/min, and powder feed rate: 15g/min.

Table 20 - Results obtained in Tests 1 and 2 using a welding current of 90A, a welding speed of 200mm/min, and a powder feed rate of 10.4 and 20g/min

Welding Current [A]	Welding Speed [mm/min]	Powder Feed Rate [g/min]	Wall Thickness [mm]	Layer Thickness [mm]	Hardness [HV 1]
90	200	10.4	5.3 ± 0.46	2.12 ± 0.09	587.70 ± 0
		20	5.1 ± 0.10	2.85 ± 0.05	586.07 ± 14.75

Initially, was tested the wall and layer thickness and the respective overlap to be used between weld beads, using these parameters. As expected, it was obtained a wall and layer thickness with approximately 5mm and 2.5mm, respectively. As such, after testing 4mm spacing between weld beads, which would lead to an overlap between them of approximately 0.5mm, it was decided to use a spacing between weld beads of 3mm, leading to an overlap of approximately 1mm. Using thirteen weld beads per layer, the cube width would be approximately 50 to 55mm. Since the parameters were kept constant throughout the production of the cube, a subsidence of the upper layer was expected. As such, a distance between layer of 3mm was maintained. Using 20 layer, the cube was expected to be 45 to 50mm high. The other process parameters were kept the same as the other tests. The depositions were made in zigzag and each time a layer was increased, the weld beads were deposited in a perpendicular orientation compared to the previous ones.

After the production of the cub, the cutting and preparation for analysis followed similar steps to those performed for the analysis of the weld beads.

3.4.1 Results

After cutting the cube it was verified that it was filled, with only one cavity in the upper part. It was also found that there was a subsidence of the layers, leading to the total height obtained being approximately 45 mm. This can be explained by the fact that deposition was carried out constantly, without any cooling time between layers, or changing the deposition parameters to compensate the reached temperatures in the layers already deposited.

The average hardness recorded in the block was approximately 540 ± 13HV. In Figure 52 are represented the hardness values registered in the cube. These values tend to remain constant throughout the block, between 520 and 540HV. At the bottom, the cube shows a slight upward trend, reaching a maximum hardness of 570HV. Immediately after transition from the cube to the base material the hardness decreases. However, given the very similar hardness values, the different layers cooling rate and the reheating phenomenal, didn't have a significant influence in the process.

The fact that the hardness remains constant throughout the entire cube can be explained by the small size of the produced part. As such, all the layers were subjected to similar thermal gradients.

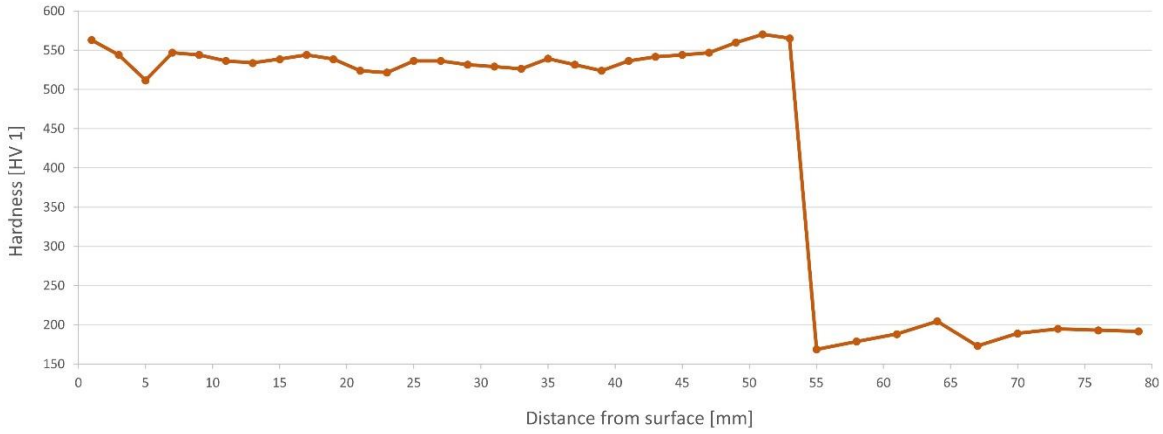

Figure 52 - Hardness variation in the cube

In the hardness variation of the plot of Figure 52 is not observed the gradual decrease in hardness as it transitions from the dilution zone to the HAZ and then to the base material. The reason for this could be the transverse cut that was made. This cut was made parallel to first layer weld beads, and possibly in the lateral or overlapping zones of them. As this is a process that does not generate a very large HAZ, the gradual hardness decrease is not visible in the measurement area.

In Figure 53 is represented the cube and the respective microstructure evolution. The structure remains similar throughout the whole measurement line. However, a

microscopic analysis using higher magnification, should be performed to analyse the grain size. This study wasn´t possible to carry out in time to present in this work.

The only defects present are a cavity in the top layer and a crack in the side. The cavity present can be caused by refusion occurring in the top, and the crack can be caused by accentuated slump on the sides.

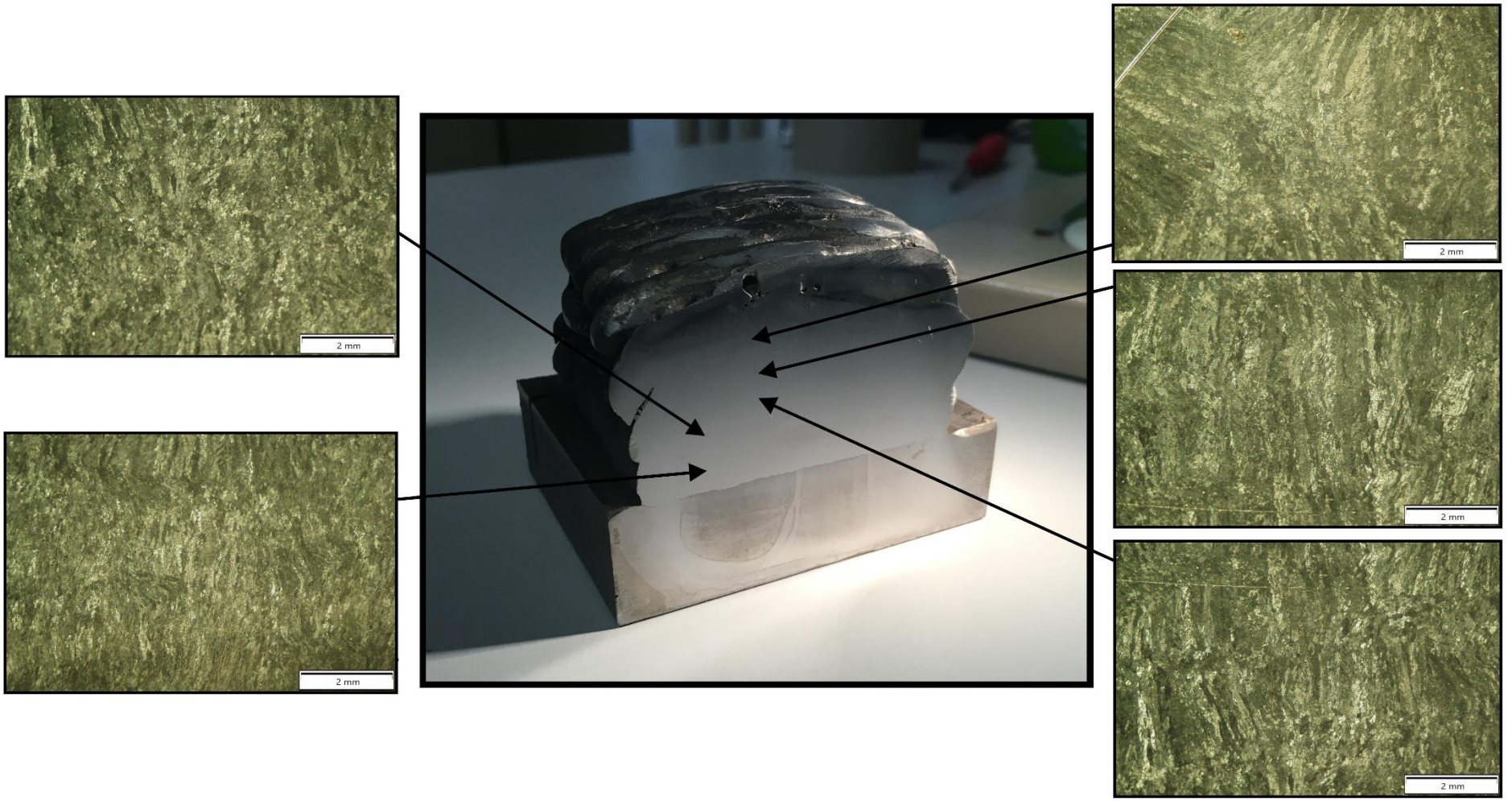

Figure 53 - Microstructure of the cube

CONCLUSIONS AND PROPOSAL FOR FUTURE STUDIES

4 Conclusions and Proposal for Future Studies

4.1 Conclusions

Additive manufacturing is gaining an increasingly important role in the industry, with enormous potential not only for prototype manufacturing, but also for repairing parts or even producing them. For the success of the process, knowledge of the process parameters and their causal relationships is fundamental. As such, the aim of this work was to investigate the influence of most important parameters in the 3DPMD and demonstrate the feasibility of producing parts.

For this, the process setup was prepared, the process parameters studied and defined. The welding current, welding speed and powder feed rate were considered the priority factors. After that, a two full factorial DOE were created and performed.

Applying the ANOVA variance test no correlation was found between process parameters. Using the *spearmen's* correlation coefficient and the main effect plots to study the influence of each factor in each response was concluded that increasing the welding speed leads to a reduction in layer and wall thickness and an increase in welding current leads to a decrease in layer thickness and an increase in wall thickness. Despite the need for further confirmation tests, it was found that the powder feed rate only affects significatively the layer thickness. Increasing the powder feed rate the layer thickness increase and the hardness decrease. These results show that the powder feed rate can be a control parameter, using it to adjust the layer thickness without changing the wall thickness. It should also be mentioned that the hardness obtained varied in a small range of values, allowing to conclude that the hardness was not much affected. Therefore, it can be concluded that there is no great significance in its variation. It was also observed that the hardness values obtained were higher than the ones estimated by the supplier. The Table 21 summarises the conclusions referred in this paragraph.

Table 21 - Summarized conclusions

		Response		
		Wall Thickness	Layer Thickness	Hardness
Parameter*	Welding Current	↑↑↑	↓↓	–
	Welding Speed	↓↓↓	↓↓↓	–
	Powder Feed Rate	–	↑↑	↑

*Parameter Increase

It was also found that, when performing slicing, attention should be paid to the quality of the weld beads produced and not only to the relationships between process parameters and responses. Excessively high current values lead to dilution values that are quite different from those typical in a PTA process. For a high welding current (150A and 170A) at a low powder feed rate (10.4g/min), the produced weld beads show a non-constant deposition, the high percentages of dilution, and the appearance of cavities. For a low welding current (70 and 90A) and low powder feed rate (10.4 g/min) the deposited beads also present defects, namely discontinuities. For a low welding current (70 and 90A) and high powder feed rate(20g/min) the depositions are irregular for the highest welding speeds (400 to 600 mm/min).

In conclusion, the perfect combination of parameters will always depend on the desired geometry in each layer. For example, a combination of parameters that leads to a thicker layer can be used for the filling, while for parts with more detail, parameters that leads to thinner layer can be chosen. Using different parameter combinations, it is possible to obtain the same layer and wall thickness, because the same heat input values can be obtained combining low welding speed with low welding current, or high welding speed with high welding current.

A geometry test was produced, showing that it is possible to produce filled parts with a constant structure, presenting hardness values approximately constant along the cross-section. The deviation that occurred in the obtained height and the expected height was due to the subsidence of the upper layers, since the process was performed with constant parameters through the layers and without using cooling time between layers.

A post-finishing machining could be applied to obtain the final part.

It is worth mentioning that with this work it was possible to deepen the knowledge about the additive manufacturing processes, in particular the 3DPMD, experiments planning and its statistical analysis, application of alternative tools to solve problems (Python programming language).

4.2 Future Studies

As a proposal for future work, to integrate a robotic arm to the process and develop a program to decompose the CAD component, with the respective variation of parameters along the layers, according to the component geometry and the properties required. For this purpose, is propose:

- Produce two overlapping weld beads;
- Microstructural study (SEM, XRD) to evaluate the effect of overlapping, in particular the grain size variation;
- Create a parameter variation matrix to serve as a basis for the deposition program;
- Deposit several layers to produce a wall, varying the parameters although the layers;
- Produce specimens from the produced wall to perform mechanical and wear tests;
- Study the influence of heat treatments to standardise the microstructure of the parts produced, if any variation is found.

The use of a thermographic camera is suggested to evaluate the respective temperature variations during the process, and thus calibrate the deposition time between layers.

BIBLIOGRAPHY AND OTHERS INFORMATIONS SOURCES

5 BIBLIOGRAPHY AND OTHERS INFORMATIONS SOURCES

[1] B. Blakey-Milner *et al.*, "Metal additive manufacturing in aerospace: A review," *Mater. Des.*, vol. 209, p. 110008, 2021, doi: 10.1016/j.matdes.2021.110008.

[2] E. Herderick, "Additive manufacturing of metals: A review," *Mater. Sci. Technol. Conf. Exhib. 2011, MS T'11*, vol. 2, no. 176252, pp. 1413–1425, 2011.

[3] J. P. Kruth, P. Mercelis, J. Van Vaerenbergh, L. Froyen, and M. Rombouts, "Binding mechanisms in selective laser sintering and selective laser melting," *Rapid Prototyp. J.*, vol. 11, no. 1, pp. 26–36, 2005, doi: 10.1108/13552540510573365.

[4] D. Bourell *et al.*, "Materials for additive manufacturing," *CIRP Ann. - Manuf. Technol.*, vol. 66, no. 2, pp. 659–681, 2017, doi: 10.1016/j.cirp.2017.05.009.

[5] L. E. Murr *et al.*, "Metal Fabrication by Additive Manufacturing Using Laser and Electron Beam Melting Technologies," *J. Mater. Sci. Technol.*, vol. 28, no. 1, pp. 1–14, 2012, doi: 10.1016/S1005-0302(12)60016-4.

[6] S. Biamino *et al.*, "Electron beam melting of Ti-48Al-2Cr-2Nb alloy: Microstructure and mechanical properties investigation," *Intermetallics*, 2011, doi: 10.1016/j.intermet.2010.11.017.

[7] M. Rombouts, J. P. Kruth, L. Froyen, and P. Mercelis, "Fundamentals of Selective Laser Melting of alloyed steel powders," *CIRP Ann.*, vol. 55, no. 1, pp. 187–192, 2006, doi: https://doi.org/10.1016/S0007-8506(07)60395-3.

[8] X. Zhou *et al.*, "3D-imaging of selective laser melting defects in a Co–Cr–Mo alloy by synchrotron radiation micro-CT," *Acta Mater.*, vol. 98, pp. 1–16, 2015, doi: https://doi.org/10.1016/j.actamat.2015.07.014.

[9] G. M. Karthik and H. S. Kim, *Heterogeneous Aspects of Additive Manufactured Metallic Parts: A Review*, vol. 27, no. 1. The Korean Institute of Metals and Materials, 2021.

[10] D.-G. Ahn, "Directed Energy Deposition (DED) Process: State of the Art," *Int. J. Precis. Eng. Manuf. Technol.*, vol. 8, 2021, doi: 10.1007/s40684-020-00302-7.

[11] M. Dalaee *et al.*, "Feasibility study in combined direct metal deposition (DMD) and plasma transfer arc welding (PTA) additive manufacturing," *Int. J. Adv. Manuf. Technol.*, vol. 106, no. 9–10, pp. 4375–4389, 2020, doi: 10.1007/s00170-019-04917-2.

[12] K. E. K. Vimal, M. Naveen Srinivas, and S. Rajak, "Wire arc additive manufacturing of aluminium alloys: A review," *Mater. Today Proc.*, vol. 41, pp. 1139–1145, 2019, doi: 10.1016/j.matpr.2020.09.153.

[13] K. Hoefer, J. Rodriguez, A. Haelsig, K. G. Abstoss, and P. Mayr, "Fabrication of SS316L to Ni80Cr20 graded structures by 3D plasma metal deposition," *Weld. World*, vol. 64, no. 8, pp. 1307–1311, 2020, doi: 10.1007/s40194-020-00870-x.

[14] J. Rodriguez, K. Hoefer, A. Haelsig, and P. Mayr, "Functionally graded SS 316l to ni-based structures produced by 3D plasma metal deposition," *Metals (Basel).*, vol. 9, no. 6, 2019, doi: 10.3390/met9060620.

[15] K. Hoefer and P. Mayr, "Additive manufacturing of titanium parts using 3d plasma

metal deposition," *Mater. Sci. Forum*, vol. 941 MSF, pp. 2137–2141, 2018, doi: 10.4028/www.scientific.net/MSF.941.2137.

[16] C. Eutectic, "Australian Castolin Eutectic Consumables and Equipment range," no. September. p. 12, 2014.

[17] C. Emmelmann, J. Kranz, D. Herzog, and E. Wycisk, "Laser Additive Manufacturing of Metals," in *Laser Technology in Biomimetics: Basics and Applications*, V. Schmidt and M. R. Belegratis, Eds. Berlin, Heidelberg: Springer Berlin Heidelberg, 2013, pp. 143–162.

[18] E. Herderick, "Additive Manufacturing of Metals : A Review," no. 176252, pp. 1413–1425, 2011.

[19] D. Herzog, V. Seyda, E. Wycisk, and C. Emmelmann, "Additive manufacturing of metals," *Acta Mater.*, vol. 117, pp. 371–392, 2016, doi: 10.1016/j.actamat.2016.07.019.

[20] I. Gibson, D. Rosen, B. Stucker, and M. Khorasani, *Additive Manufacturing Technologies*, 3rd ed. Springer, 2021.

[21] E. M. Igor Yadroitsev, Ina Yadroitsava, Anton Du Plessis, *Fundamentals of Laser Powder Bed Fusion of Metals*, 1st ed. Elsevier, 2021.

[22] DMG MORI, "Additive Manufacturing:Reinvent your Metal Production."

[23] J. Zhang, B. Song, Q. Wei, D. Bourell, and Y. Shi, "A review of selective laser melting of aluminum alloys : Processing, microstructure, property and developing trends," *J. Mater. Sci. Technol.*, vol. 35, no. 2, pp. 270–284, 2019, doi: 10.1016/j.jmst.2018.09.004.

[24] M. Baumers, P. Dickens, C. Tuck, and R. Hague, "The cost of additive manufacturing: Machine productivity, economies of scale and technology-push," *Technol. Forecast. Soc. Change*, vol. 102, pp. 193–201, 2016, doi: 10.1016/j.techfore.2015.02.015.

[25] J. Kranz, D. Herzog, and C. Emmelmann, "Design guidelines for laser additive manufacturing of lightweight structures in TiAl6V4," *J. Laser Appl.*, 2015, doi: 10.2351/1.4885235.

[26] A. A. Shapiro *et al.*, "Additive manufacturing for aerospace flight applications," *J. Spacecr. Rockets*, vol. 53, no. 5, 2016, doi: 10.2514/1.A33544.

[27] F. Kerstens, A. Cervone, and P. Gradl, "End to end process evaluation for additively manufactured liquid rocket engine thrust chambers," *Acta Astronautica*, vol. 182. pp. 454–465, 2021, doi: 10.1016/j.actaastro.2021.02.034.

[28] H. Bikas, P. Stavropoulos, and G. Chryssolouris, "Additive manufacturing methods and modeling approaches: A critical review," *Int. J. Adv. Manuf. Technol.*, 2016, doi: 10.1007/s00170-015-7576-2.

[29] E. Brandl, F. Palm, V. Michailov, B. Viehweger, and C. Leyens, "Mechanical properties of additive manufactured titanium (Ti-6Al-4V) blocks deposited by a solid-state laser and wire," *Mater. Des.*, vol. 32, no. 10, pp. 4665–4675, 2011, doi: 10.1016/j.matdes.2011.06.062.

[30] W. E. Frazier, "Metal Additive Manufacturing : A Review," vol. 23, no. June, pp. 1917–1928, 2014, doi: 10.1007/s11665-014-0958-z.

[31] G. Tapia and A. Elwany, "A Review on Process Monitoring and Control in Metal-Based Additive Manufacturing," *J. Manuf. Sci. Eng. Trans. ASME*, vol. 136, no. 6, 2014, doi: 10.1115/1.4028540.

[32] Z. Y. Chua, I. H. Ahn, and S. K. Moon, "Process monitoring and inspection systems

in metal additive manufacturing: Status and applications," *Int. J. Precis. Eng. Manuf. - Green Technol.*, 2017, doi: 10.1007/s40684-017-0029-7.

[33] C. Y. Yap *et al.*, "Review of selective laser melting: Materials and applications," *Appl. Phys. Rev.*, vol. 2, no. 4, 2015, doi: 10.1063/1.4935926.

[34] O. D. Neikov, "Powders for Additive Manufacturing Processing," in *Handbook of Non-Ferrous Metal Powders*, 2nd ed., O. D. Neikov, S. S. Naboychenko, and N. A. Yefimov, Eds. Oxford: Elsevier, 2019, pp. 373–399.

[35] Y. P. Kathuria, "Microstructuring by selective laser sintering of metallic powder," *Surf. Coatings Technol.*, vol. 116–119, pp. 643–647, 1999, doi: 10.1016/S0257-8972(99)00266-2.

[36] K. Amato, "Comparison of Microstructures and Properties for a Ni-Base Superalloy (Alloy 625) Fabricated by Electron Beam Melting," *J. Mater. Sci. Res.*, vol. 1, no. 2, 2012, doi: 10.5539/jmsr.v1n2p3.

[37] G. Additive, "Inside Electron beam melting." p. 10, 2007, doi: 10.31399/asm.hb.v15.a0005204.

[38] D. Cormier, O. Harrysson, and H. West, "Characterization of H13 steel produced via electron beam melting," *Rapid Prototyp. J.*, vol. 10, no. 1, pp. 35–41, 2004, doi: 10.1108/13552540410512516.

[39] B. Van der Schueren and J. P. Kruth, "Powder deposition in selective metal powder sintering," *Rapid Prototyp. J.*, vol. 1, no. 3, pp. 23–31, 1995, doi: 10.1108/13552549510094241.

[40] J. L. Brackpool, "The Effect of Material Characteristics on the Compaction Behaviour of Metal Powders," in *Modern Developments in Powder Metallurgy*, 1971, pp. 423–435.

[41] W. H. Organization, "Bulk Density And Tapped Density Of Powders," no. March. World Health Organization, p. 6, 2012.

[42] Aniwaa, "Concept Laser M3 linear overview." https://www.aniwaa.com/product/3d-printers/concept-laser-m3-linear/ (accessed Sep. 22, 2021).

[43] K. Maxey, "Concept Laser M3 Linear," 2015. https://www.engineering.com/story/concept-laser-m3-linear (accessed Sep. 22, 2021).

[44] A. M. and Design, "Renishaw AM250 additive manufacturing system." https://www.aerospacemanufacturinganddesign.com/article/renishaw-am250-additive-manufacturing-system-071815/ (accessed Sep. 22, 2021).

[45] "Phenix PXL." https://www.aniwaa.com/product/3d-printers/3d-systems-phenix-pxl/ (accessed Sep. 22, 2021).

[46] P. Systems, "Additive manufacturing systems using laser sintering." [Online]. Available: http://brochure.copiercatalog.com/3d-systems/brochure_phenix_systems_gb_2012.pdf.

[47] S. GmbH, "Laser Beam Melting System SLM 250 HL." pp. 2–3, 2012, [Online]. Available: www.slm-solutions.com.

[48] A. E. Systems, "Arcam EBM S12." [Online]. Available: www.arcam.com.

[49] M. Simonelli, Y. Y. Tse, and C. Tuck, "A Effect of the build orientation on the mechanical properties and fracture modes of SLM Ti – 6Al – 4V," *Mater. Sci. Eng.*, vol. 616, pp. 1–11, 2014, doi: 10.1016/j.msea.2014.07.086.

[50] N. Hrabe and T. Quinn, “Effects of processing on microstructure and mechanical properties of a titanium alloy (Ti–6Al–4V) fabricated using electron beam melting (EBM), Part 2: Energy input, orientation, and location,” *Mater. Sci. Eng.*, vol. 573, pp. 271–277, 2013, doi: https://doi.org/10.1016/j.msea.2013.02.065.

[51] P. Edwards, T. Motors, and M. Ramulu, “Electron Beam Additive Manufacturing of Titanium Components : Properties and Performance,” no. December, 2013, doi: 10.1115/1.4025773.

[52] Y. Zhai, H. Galarraga, and D. A. Lados, “Microstructure Evolution , Tensile Properties , and Fatigue Damage Mechanisms in Ti-6Al-4V Alloys Fabricated by Two Additive Manufacturing Techniques,” *Procedia Eng.*, vol. 114, pp. 658–666, 2015, doi: 10.1016/j.proeng.2015.08.007.

[53] S. L. Sing, J. An, W. Y. Yeong, and F. E. Wiria, “Laser and Electron-Beam Powder-Bed Additive Manufacturing of Metallic Implants : A Review on Processes , Materials and Designs,” *J. Orthop.*, no. March, p. 17, 2016, doi: 10.1002/jor.23075.

[54] W. J. Sames, F. A. List, S. Pannala, R. R. Dehoff, and S. S. Babu, “The metallurgy and processing science of metal additive manufacturing,” *Int. Mater. Rev.*, vol. 61, no. 5, pp. 315–360, 2016, doi: 10.1080/09506608.2015.1116649.

[55] D. Svetlizky *et al.*, “Directed energy deposition (DED) additive manufacturing: Physical characteristics, defects, challenges and applications,” *Mater. Today*, vol. 49, no. 10, pp. 271–295, 2021, doi: 10.1016/j.mattod.2021.03.020.

[56] G. Tapia and A. Elwany, “A Review on Process Monitoring and Control in Metal-Based Additive Manufacturing,” *Journal of Manufacturing Science and Engineering, Transactions of the ASME*. 2014, doi: 10.1115/1.4028540.

[57] E. M. Perez-Soriano, E. Ariza, C. Arevalo, I. Montealegre-Melendez, M. Kitzmantel, and E. Neubauer, “Processing by additive manufacturing based on plasma transferred arc of hastelloy in air and argon atmosphere,” *Metals (Basel).*, vol. 10, no. 2, 2020, doi: 10.3390/met10020200.

[58] S. W. Williams, F. Martina, A. C. Addison, J. Ding, G. Pardal, and P. Colegrove, “Wire + Arc additive manufacturing,” *Mater. Sci. Technol. (United Kingdom)*, vol. 32, no. 7, pp. 641–647, 2016, doi: 10.1179/1743284715Y.0000000073.

[59] J. Gu, B. Cong, J. Ding, S. W. Williams, and Y. Zhai, “Wire+Arc additive manufacturing of aluminium,” *25th Annu. Int. Solid Free. Fabr. Symp.*, pp. 451–458, 2014.

[60] T. DebRoy *et al.*, “Additive manufacturing of metallic components – Process, structure and properties,” *Prog. Mater. Sci.*, vol. 92, pp. 112–224, 2018, doi: 10.1016/j.pmatsci.2017.10.001.

[61] H. Zhu *et al.*, “The characterisation and formation of novel microstructural features in a Ti−Nb−Zr−Mo−Sn alloy manufactured by Laser Engineered Net Shaping (LENS),” *Addit. Manuf.*, vol. 37, no. November 2020, 2021, doi: 10.1016/j.addma.2020.101705.

[62] K. Hoefer, A. Nitsche, A. Haelsig, and P. Mayr, “Manufacturing of titanium components with 3DPMD,” *Metals (Basel).*, vol. 9, no. 5, 2019, doi: 10.3390/met9050562.

[63] K. Hoefer, A. Nitsche, K. G. Abstoss, G. Ertugrul, A. Haelsig, and P. Mayr, “Multi-material Additive Manufacturing by 3D Plasma Metal Deposition for Graded Structures of Super Duplex Alloy 1.4410 and the Austenitic Corrosion Resistant Alloy 1.4404,” *Jom*, vol. 71, no. 4, pp. 1554–1559, 2019, doi: 10.1007/s11837-019-03356-4.

[64] D. Bond and A. S. C. M. D'Oliveira, "Effect of current and atomized grain size distribution on the solidification of plasma transferred arc coatings," *Mater. Res.*, vol. 15, no. 5, pp. 770–774, 2012, doi: 10.1590/S1516-14392012005000101.

[65] A. K. Lakshminarayanan, V. Balasubramanian, R. Varahamoorthy, and S. Babu, "Predicting the dilution of plasma transferred arc hardfacing of stellite on carbon steel using response surface methodology," *Met. Mater. Int.*, vol. 14, no. 6, pp. 779–789, 2008, doi: 10.3365/met.mat.2008.12.779.

[66] A. Gatto, E. Bassoli, and M. Fornari, "Plasma Transferred Arc deposition of powdered high performances alloys: Process parameters optimisation as a function of alloy and geometrical configuration," *Surf. Coatings Technol.*, vol. 187, no. 2–3, pp. 265–271, 2004, doi: 10.1016/j.surfcoat.2004.02.013.

[67] W. Xibao and L. Hua, "Metal Powder Thermal Behaviour During the Plasma Transferred-Arc Surfacing Process," *Surf. Coatings Technol.*, vol. 106, no. 2–3, pp. 156–161, 1998, doi: 10.1016/S0257-8972(98)00521-0.

[68] R. H. G. e Silva and J. C. Dutra, "Processo PTA-P - Uma revisão da literatura como base para inovações. Parte 1 de 2: Elementos construtivos," *Soldag. e Insp.*, 2012, doi: 10.1590/S0104-92242012000100011.

[69] K. Alaluss and P. Mayr, "Additive manufacturing of complex components through 3D plasma metal deposition—A simulative approach," *Metals (Basel).*, vol. 9, no. 5, pp. 1–19, 2019, doi: 10.3390/met9050574.

[70] K. Hoefer, "Correlations between Process and Geometric Parameters in Additive Manufacturing of Austenitic Stainless Steel Components Using 3DPMD," *Appl. Sci.*, pp. 0–7, 2021.

[71] S.Kou and T. DebRoy, "Heat Flow in Welding," in *Welding HandBook*, 9th ed., Miami: Society A, 2001.

[72] K. Hoefer, "3D plasma metal deposition for processing multi material Titanium parts," *Weld. Int.*, vol. 35, no. 1–3, pp. 12–15, 2021, doi: 10.1080/09507116.2021.1890988.

[73] B. Vrancken, L. Thijs, J. P. Kruth, and J. Van Humbeeck, "Microstructure and mechanical properties of a novel $β$ titanium metallic composite by selective laser melting," *Acta Mater.*, vol. 68, pp. 150–158, 2014, doi: 10.1016/j.actamat.2014.01.018.

[74] J. Martin, *Materials for engineering*. Woodhead Publishing, 2006.

[75] Q. Han *et al.*, "Laser powder bed fusion of Hastelloy X: Effects of hot isostatic pressing and the hot cracking mechanism," *Mater. Sci. Eng. A*, vol. 732, no. July, pp. 228–239, 2018, doi: 10.1016/j.msea.2018.07.008.

[76] M. Balasubramanian, M. V. Choudary, A. Nagaraja, and K. O. C. Sai, "Cold metal transfer process - A review," *Mater. Today Proc.*, vol. 33, pp. 543–549, 2020, doi: 10.1016/j.matpr.2020.05.225.

[77] J. Bi, J. Shen, S. Hu, Y. Zhen, F. Yin, and X. Bu, "Microstructure and mechanical properties of AZ91 Mg alloy fabricated by cold metal transfer additive manufacturing," *Mater. Lett.*, vol. 276, pp. 10–13, 2020, doi: 10.1016/j.matlet.2020.128185.

[78] C. Zhang, Y. Li, M. Gao, and X. Zeng, "Wire arc additive manufacturing of Al-6Mg alloy using variable polarity cold metal transfer arc as power source," *Mater. Sci. Eng. A*, vol. 711, no. August 2017, pp. 415–423, 2018, doi: 10.1016/j.msea.2017.11.084.

[79] G. Posch, K. Chladil, and H. Chladil, "Material properties of CMT—metal additive

manufactured duplex stainless steel blade-like geometries," *Weld. World*, vol. 61, no. 5, pp. 873–882, 2017, doi: 10.1007/s40194-017-0474-5.

[80] Y. Zhong, Z. Zheng, J. Li, and C. Wang, "Fabrication of 316L nuclear nozzles on the main pipeline with large curvature by CMT wire arc additive manufacturing and self-developed slicing algorithm," *Mater. Sci. Eng. A*, vol. 820, no. May, p. 141539, 2021, doi: 10.1016/j.msea.2021.141539.

[81] V. A. De Meneses, J. F. P. Gomes, and A. Scotti, "The effect of metal transfer stability (spattering) on fume generation, morphology and composition in short-circuit MAG welding," *J. Mater. Process. Technol.*, vol. 214, no. 7, pp. 1388–1397, 2014, doi: 10.1016/j.jmatprotec.2014.02.012.

[82] K. Hoefer, A. Haelsig, and P. Mayr, "Arc-based additive manufacturing of steel components—comparison of wire- and powder-based variants," *Weld. World*, vol. 62, no. 2, pp. 243–247, 2018, doi: 10.1007/s40194-017-0527-9.

[83] K. Höfer, "Qualification of the plasma powder build-up welding process for the generative production of components of the alloy 1.4404," Ph.D. Thesis, Chemnitz University of Technology, Chemnitz, Germany, 2021.

[84] J. Antoy, *Design of Experiments for Engineers and Scientists*, 2nd ed. Elsevier, 2014.

[85] A. Rafidah, A. Nurulhuda, A. Azrina, Y. Suhaila, I. S. Anwar, and R. A. Syafiq, "Comparison design of experiment (DOE): Taguchi method and full factorial design in surface roughness," 2014, doi: 10.4028/www.scientific.net/AMM.660.275.

[86] Castolin, "Technical data sheet 'Alliage en poudre atomisée à Eutroloy 16604,'" p. 1, 2021.

[87] M. Demiral, F. Abbassi, T. Saracyakupoglu, and M. Habibi, "Damage analysis of a CFRP cross-ply laminate subjected to abrasive water jet cutting," *Alexandria Eng. J.*, vol. 61, no. 10, pp. 7669–7684, 2022, doi: 10.1016/j.aej.2022.01.018.

[88] C. Joel, T. Jeyapoovan, and P. Praneeth Kumar, "Experimentation and optimization of cutting parameters of abrasive jet cutting on AA6082 through response surface methodology," *Mater. Today Proc.*, vol. 44, pp. 3564–3570, 2021, doi: 10.1016/j.matpr.2020.09.452.

[89] M. ElTobgy, E. G. Ng, and M. A. Elbestawi, "Modelling of abrasive waterjet machining: A new approach," *CIRP Ann. - Manuf. Technol.*, vol. 54, no. 1, pp. 285–288, 2005, doi: 10.1016/s0007-8506(07)60104-8.

[90] Cobram Water Plasma Jet Cutting & Engineering, "Water Jet Cutting." https://www.cobramwaterjet.com.au/waterjet-cutting.html (accessed May 05, 2022).

[91] ASTM E3-11, "Standard Guide for Preparation of Metallographic Specimens 1." ASTM International, West Conshohocken, PA, USA, 2011.

[92] EN ISO 6507-1, "Metallic materials - Vickers hardness test - Part 1: Test method." NSAI Standards, 2018.

[93] S. F. C. Ehsan Toyserkani, Amir Khajepour, *Laser Cladding*, 1st ed. CRC Press, 2005.

[94] M. Schneider, "Laser clading with powder effect of some machining parameters on clad properties," University of Twente, Enschede, 1998.

[95] S. Jhavar, C. P. Paul, and N. K. Jain, "Micro-Plasma Transferred Arc Additive Manufacturing for Die and Mold Surface Remanufacturing," *Jom*, vol. 68, no. 7, pp. 1801–1809, 2016, doi: 10.1007/s11837-016-1932-z.

[96] “OpenCv.” https://opencv.org/ (accessed Aug. 10, 2022).
[97] “Matplotlib.” https://matplotlib.org/ (accessed Aug. 10, 2022).

APPENDIX

6 APPENDIX

6.1 Assembly of Plasma Transferred Arc Machine

6.2 Eutronic GAP® 3511 Synergic

Eutronic GAP® 3511 Synergic	ESC: 763890
Supply voltage:	3x 400V ±10% 3x 460V ±5%
Supply frequency:	50/60 Hz
Supply fuse:	32 A
Max. power consumption:	20 kVA
Maximum rated value of the power supply current	32 A
Effective value of the maximum power supply current	25 A
Cos phi:	0.99
Max. welding current (35% ED):	350 A
Max. welding current (60% ED):	280 A
Max. welding current (100% ED):	250 A
Pilot current (100% ED):	30 A
Amperage range for plasma and TIG welding	10 A ÷ 350 A
Amperage range for electrode welding	10 A ÷ 280 A
Amperage range for pilot current	2 A ÷ 50 A
Open Circuit Voltage - pilot inverter:	95 V DC
Open Circuit Voltage - main inverter:	95 V DC
Dimensions (L x W x H):	815 x 445 x 635 mm
Weight:	105 kg

6.3 RC-H manual remote control

RC-H manual remote control	ESC: 260231
including 8 metres connecting cable.	

6.4 Cooling GAP Chiller

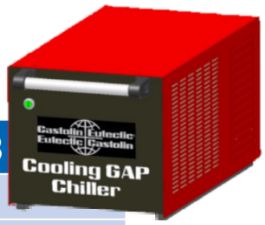

Cooling GAP® Chiller	ESC: 754273
Weight:	50 kg
Dimensions (L x W x H):	915 x 445 x 400 mm
Cooling with integrated chiller.	

6.5 Powder Feeder EP2

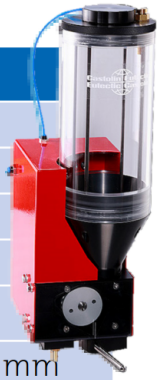

Powder Feeder EP2	ESC: 260229
Carrier gas:	Ar, Ar-H2
Carrier gas flow rate:	0 - 4 l/min
Powder reservoir:	2 l capacity
Protection class:	IP 23
Weight (without powder):	7,5 kg
Dimensions (L x W x H):	200 x 170 x 470 mm
Powder feed rate 3 - 120 g/min, depending on feeding wheel configuration, torch, anode and powder density.	

6.6 Base Material Chemical Composition

Measurement Results

Instrument 78A1038
Sample
Alloy FE_100 Mode Element Concentration

	C [%]	Si [%]	Mn [%]	P [%]	S [%]	Cr [%]	Mo [%]
1	0,4305	0,2454	0,6920	0,0115	0,0052	0,0259	0,0068
2	0,4135	0,2419	0,6931	0,0108	0,0036	0,0244	0,0067
3	0,4017	0,2405	0,7009	0,0113	0,0047	0,0242	0,0066
4	0,4074	0,2324	0,6389	0,0077	0,0011	0,0224	0,0066
5	0,4112	0,2415	0,6718	0,0099	0,0034	0,0230	0,0069
Ø	**0,4129**	**0,2403**	**0,6793**	**0,0102**	**0,0036**	**0,0240**	**0,0067**

	Ni [%]	Al [%]	Co [%]	Cu [%]	Nb [%]	Ti [%]	V [%]
1	0,0128	0,0292	0,0007	0,0126	0,0007	0,0017	0,0030
2	0,0124	0,0294	0,0007	0,0127	0,0006	0,0016	0,0029
3	0,0126	0,0288	0,0007	0,0127	<0,0005	0,0018	0,0030
4	0,0113	0,0314	0,0006	0,0121	<0,0005	0,0010	0,0026
5	0,0115	0,0303	0,0006	0,0125	0,0005	0,0014	0,0028
Ø	**0,0121**	**0,0298**	**0,0006**	**0,0125**	**0,0006**	**0,0015**	**0,0029**

	W [%]	Pb [%]	Sn [%]	Zr [%]	Zn [%]	N [%]	Se [%]
1	<0,0020	<0,0005	0,0008	<0,0005	0,0018	0,0091	<0,0010
2	<0,0020	<0,0005	0,0008	<0,0005	0,0017	0,0091	<0,0010
3	<0,0020	<0,0005	0,0010	<0,0005	0,0018	0,0096	<0,0010
4	<0,0020	0,0005	0,0010	<0,0005	0,0017	0,0032	<0,0010
5	<0,0020	<0,0005	0,0011	<0,0005	0,0018	<0,0010	<0,0010
Ø	**<0,0020**	**0,0005**	**0,0009**	**<0,0005**	**0,0018**	**0,0064**	**<0,0010**

	B [%]	Ca [%]	Bi [%]	As [%]	Ta [%]	Sb [%]	Fe [%]
1	0,0005	<0,0001	<0,0005	0,0011	0,0403	<0,0005	98,46
2	0,0004	<0,0001	<0,0005	0,0013	0,0411	0,0009	98,49
3	0,0004	<0,0001	<0,0005	0,0016	0,0404	0,0008	98,49
4	0,0004	<0,0001	<0,0005	0,0011	0,0404	0,0015	98,57
5	0,0005	<0,0001	<0,0005	0,0008	0,0401	0,0011	98,52
Ø	**0,0004**	**<0,0001**	**<0,0005**	**0,0011**	**0,0404**	**0,0010**	**98,51**

6.7 Powder Eutroloy 16604 Specifications

welding - wear solutions - automation

Plasma Transferred Arc (PTA) Welding

EuTroLoy® Plasma Transferred Arc Powders




Product	Product Type	Applications / Features	Properties
EuTroLoy® 16494	Self-fluxing Ni base alloy	GAP welding process, oxidation resistant up to 800°C. Corrosion resistant and has low coefficient of sliding metal friction. High adhesive strength. Typical applications: slide valves for oil and steam, glass making tools, foundry tools,	~39 to 42 HRC 0.4 C, 10 Cr, 1.8 B, 2.7 Si, max 0.2 Fe, Bal Ni. Good resistance to high temperature (800° C) Good metal to metal friction properties
EuTroLoy® 16495	Self-fluxing Ni base alloy	GAP welding process, high temperature oxidation and corrosion resistance. Typical applications: Steam and oil/gas valve shutters, slide valves, pump impellers, wear rings, glass making components.	~50 HRC 0.5 C, 12 Cr, 2.2 B, 3.2 Si, max 0.2 Fe, Bal Ni Good resistance to high temperature oxidation and corrosion, (750°C). Good metal to metal friction properties.
EuTroLoy® 16496	Self-fluxing Ni base alloy	Hardfacing of seal surfaces in valves, sliding seals and slide ways, forming tools, valves, valve flaps, pump rotors, cams and worm screw parts.	~60 HRC 0.7 C, 16 Cr, 3.3 B, 4.2 Si, max 0.3 Fe, Bal Ni Good resistance to high temperature oxidation and abrasion, (700°C). Good friction properties.
EuTroLoy® 16604	Alloy Fe-Co-Cr-Mo	Tools for hot and cold metal shaping: clipping bed, rolling mills, bending machines, sealing joints. Excellent buttering layer before coating with cobalt based alloys.	~45 HRC Work-hardening deposit with very fine martensitic structure. Excellent resistance to heat, thermal shock and corrosion. Good resistance to cracking.
EuTroLoy® 16606	Alloy Fe-W-Cr-Mo-V	Temperature-stressed dies and mandrels, cutting tools, also for natural fibres, punching, compression moulding and drawing dies, forging inserts, worm screw parts, valves, barrel extruders.	~58 HRC Martensitic weld metal based on cold work tool steel. Wear-resistant to abrasion and fatigue stress as well as when subjected to a combination of abrasion and fatigue stress. Hot wear resistant. Good tempering properties. Heat treatable.
EuTroLoy® 16625	Alloy Ni-Cr-Mo-Nb-Fe	Marine engine components, power plant components, installations on drilling rigs, valve components for mineral oil, tools for underwater work and low-temperature equipment.	~210 HV30 High ductility. Very good corrosion resistance (e.g. seawater). Tough at subzero temperatures, suitable for cryogenic use.
EuTroLoy® 16800	Alloy Ni-Mo-Cr-W	Mixer arms, components in the paper industry, hot shears, hot trimming dies, extrusion dies, valve seats, pump components in the chemical industry.	~260 HV30 Very high resistance to inter crystalline corrosion, interfacial corrosion and stress corrosion cracking. Excellent corrosion resistance to oxidising media such as nitric, phosphoric, sulphuric and sulphurous acid. Also resistant to ethanoic, lactic, citric and fatty acids, caustic soda as well as media containing chloride.
EuTroLoy® PG 6503	Ni-B-Si-Fe alloy and tungsten carbide	Dragline bucket wear components, ground engaging tool protection. Decanting and transport screw. Mixer pieces. Drilling tools. Brick or tile dies. Protective sleeves. Wood-working tools.	~60 HRC 60% tungsten carbides. Excellent resistance to abrasion.

Many more powder alloys are available upon request. Please ask your local Representative.

Alliage en poudre atomisée à gaz - EuTroLoyÒ 16604

Pour utilisation avec le procédé plasma d'arc transféré PTA

Description Alliage en poudre pour des revêtements réalisés avec le procé-dé plasma d'arc transféré (PTA). Les revêtements, réalisés avec EuTroLoy 16604 possèdent une résistance élevée à l'oxydation et à la formation de calamine. Par ailleurs ils se caractérisent par une bonne aptitude au glissement et une haute résistance à l'abrasion au contact métal/métal. Le revê-tement est non magnétique et résiste aux chocs thermiques. Par écrouissage, la dureté peut augmenter. EuTroLoy 16604 est une poudre pré-alliée. Elle est élaborée par atomisation gazeuse pour obtenir une forme sphérique et pour assurer un haut niveau de pureté avec une basse teneur en oxygène dissout dans les grains de poudre. La forme sphérique et la granulométrie des poudres sont ajus-tées de façon précise et adaptées aux divers équipements pour obtenir des débits réguliers.

Caractéristiques techniques Composition nominale (en % de la masse) : Max. 0,2C-15Cr-15Co-2,5Mo - base Fe

Morphologie : Poudre pré-alliée, homogène, composée de grains sphériques de composition uniforme.

Minimum Nominale Dureté hors dilution(HRC): 38 to 42

Température de service maximale (°C): ≈650

Applications Outils de formage des métaux à chaud et à froid: matrices d'ébavurage, plieuses. Composants de vanne. Joints d'étanchéité, etc. Sous-couche avent revêtement avec les alliages à base cobalt

Procédure d'utilisation

Préparation Les surfaces à revêtir doivent être propres, exemptes de toute trace d'oxydes et de contamination. Au préalable, enlever tout dépôt résiduel ainsi que le métal fissuré ou affecté par grippage, fatigue, corrosion, etc.

Préchauffage En principe, *EuTroLoy 16604* ne requiert pas de préchauffage. Toutefois, un préchauffage peut s'avérer nécessaire selon la composition chimique, la taille et la forme du métal de base. Les sous-couches réalisées avec des alliages à base de nickel diminuent considérablement la dureté du revêtement.

Refroidissement Le refroidissement doit être lent à l'abri des courants d'air dans un bac rempli de vermiculite ou contrôlé dans un four.

Technique de soudage Veiller impérativement à maintenir une dilution.

* Datasheet supplied by castolin

6.8 Results of Test 1 and 2

Test 1 (Powder Feed Rate: 10.4 g/min)							
Welding Current [A]	**Welding Speed [mm/min]**	**Wall Thickness [mm]**	**ST**	**Layer Thickness [mm]**	**ST**	**Hardness [HV 1]**	**ST**
70	100	4,68	0,29	3,05	0,22	617,75	6,25
	200	4,36	0,26	2,68	0,15	612,67	10,14
	300	3,46	0,25	1,64	0,20	526,40	0,00
	400	3,16	0,29	1,58	0,12	659,40	11,39
	500	2,00	0,23	1,36	0,24	658,55	1,85
	600	2,85	0,25	1,27	0,16	615,27	10,92
90	100	7,75	0,21	3,00	0,00	608,60	9,02
	200	5,30	0,46	2,12	0,10	587,70	0,00
	300	4,11	0,49	1,66	0,12	653,73	11,10
	400	3,88	0,28	1,41	0,14	686,23	10,89
	500	3,10	0,23	1,24	0,15	657,03	5,59
	600	3,20	0,40	1,24	0,15	605,70	12,10
110	100	8,93	0,37	2,78	0,24	673,23	1,72
	200	7,84	0,44	2,10	0,32	674,43	5,04
	300	6,25	0,47	1,34	0,15	663,90	0,00
	400	5,49	0,26	0,81	0,08	644,57	1,58
	500	4,81	0,45	0,68	0,10	617,83	4,41
	600	4,25	0,50	0,58	0,04	600,70	14,28
130	100	10,19	0,24	1,66	0,19	651,13	8,45
	200	8,23	0,44	1,20	0,18	630,43	4,57
	300	7,69	0,36	0,84	0,04	625,10	1,49
	400	6,26	0,15	0,56	0,07	505,77	3,91
	500	5,66	0,28	0,49	0,06	554,58	10,77
	600	4,95	0,29	0,41	0,03	581,60	10,08
150	100	11,98	0,17	1,46	0,03	642,40	3,11
	200	9,76	0,37	1,04	0,09	627,20	3,20
	300	8,04	0,39	0,80	0,08	570,90	11,88
	400	6,09	0,43	0,87	0,13	502,03	7,56
	500	5,11	0,25	0,77	0,08	563,40	0,00
	600	4,49	0,19	0,75	0,09	536,45	7,55
170	100	13,59	0,18	1,38	0,06	642,47	7,87
	200	10,57	0,50	1,04	0,11	623,10	11,65
	300	8,32	0,33	1,02	0,08	616,10	4,70
	400	6,38	0,21	1,00	0,24	649,03	4,23
	500	5,22	0,09	0,77	0,11	672,20	12,16
	600	2,57	0,00	0,27	0,00	691,47	9,65

Test 2 (Powder Feed Rate: 20 g/min)							
Welding Current [A]	**Welding Speed [mm/min]**	**Wall Thickness [mm]**	**ST**	**Layer Thickness [mm]**	**ST**	**Hardness [HV 1]**	**ST**
70	100	5,57	0,16	3,53	0,25	524,80	5,66
	200	3,97	0,21	2,38	0,03	537,18	10,20
	300	3,53	0,23	1,88	0,12	524,98	8,27
	400	3,52	0,24	2,27	0,14	560,73	8,30
	500	3,32	0,29	1,19	0,04	546,60	0,00
	600	2,92	0,32	1,14	0,24	541,25	2,55
90	100	6,61	0,08	4,10	0,10	596,67	11,07
	200	5,10	0,10	2,85	0,05	586,07	14,75
	300	4,17	0,24	2,20	0,20	539,77	5,99
	400	3,85	0,36	2,10	0,29	627,40	11,45
	500	3,65	0,22	1,83	0,20	546,73	10,61
	600	3,07	0,09	1,60	0,16	533,07	6,50
110	100	8,87	0,09	4,28	0,10	573,65	11,15
	200	7,13	0,41	2,27	0,19	618,00	0,10
	300	7,03	0,33	1,67	0,09	568,93	7,91
	400	6,27	0,25	1,37	0,05	558,10	5,47
	500	6,20	0,33	0,88	0,08	559,80	2,20
	600	5,33	0,47	0,88	0,08	582,75	8,02
130	100	9,42	0,56	3,48	0,18	641,85	4,95
	200	8,13	0,19	2,10	0,11	652,50	5,75
	300	7,47	0,19	1,60	0,11	583,90	5,37
	400	5,68	0,06	1,40	0,06	558,55	12,05
	500	5,34	0,16	1,17	0,04	584,80	0,00
	600	5,26	0,29	1,07	0,06	587,03	15,85
150	100	12,05	0,59	2,95	0,16	569,83	10,74
	200	9,78	0,56	2,02	0,06	606,40	2,83
	300	7,09	0,42	1,74	0,06	581,52	11,24
	400	6,22	0,31	1,44	0,11	555,30	11,94
	500	5,51	0,11	1,23	0,05	572,57	5,71
	600	5,37	0,19	1,04	0,03	681,63	7,73
170	100	13,36	0,41	2,90	0,00	567,07	3,41
	200	9,79	0,40	1,99	0,04	563,40	4,59
	300	8,25	0,04	1,44	0,07	586,80	5,95
	400	7,17	0,22	1,29	0,05	558,30	13,72
	500	6,25	0,12	1,14	0,02	569,40	6,90
	600	5,69	0,40	0,96	0,43	659,05	18,85

6.9 Dilution Percentage Calculation Example

Dilution Percentagem Calculation

In [1]:
```
#Required libraries
import cv2
import matplotlib.pyplot as plt
```

1) Read the Image of weld bead

In [2]:
```
#Read the image of the weld bead
WeldBead = cv2.imread("C:\\Users\\dem\\OneDrive - Instituto Superior de Engenharia do Porto\\Documents\\2.MEM\\7.T

#Display the image readed
plt.imshow(WeldBead[:,:,::-1])
plt.title("Weld Bead 1_Original Image", fontsize= 18, y=0.85)
plt.axis("off");
```

2) Process the image

In order to make it easier to locate the contours of the image by using the function "cv2.findContours()".

In [3]:
```
#Copy the original image
WeldBead_copy = WeldBead.copy()
#Convert the image to black&white
WeldBead_gray = cv2.cvtColor(WeldBead_copy, cv2.COLOR_BGR2GRAY)
```

In [4]:
```
# Apply Tozero thresholding
ret, WeldBead_gray_thresh = cv2.threshold(WeldBead_gray, 254, 255, cv2.THRESH_TOZERO)
```

In [5]:
```
#Invert the colours
WeldBead_gray_invert = cv2.bitwise_not(WeldBead_gray_thresh)
```

In [6]:
```
#Display the in results in sequence using the function of matplotlib plt.subplot
titles = ["Weld Bead 1_Black&White","Weld Bead 1_Thresholding Tozero","Weld Bead 1_Inverted"]
images = [WeldBead_gray, WeldBead_gray_thresh, WeldBead_gray_invert]
plt.figure(figsize=[15,15])
for i in range(3):
    plt.subplot(1, 3, i+1)
    plt.imshow(images[i],'gray',vmin=0,vmax=255)
    plt.title(titles[i], fontsize= 18)
    plt.xticks([]),plt.yticks([]) #Axis off
    plt.tight_layout();
```

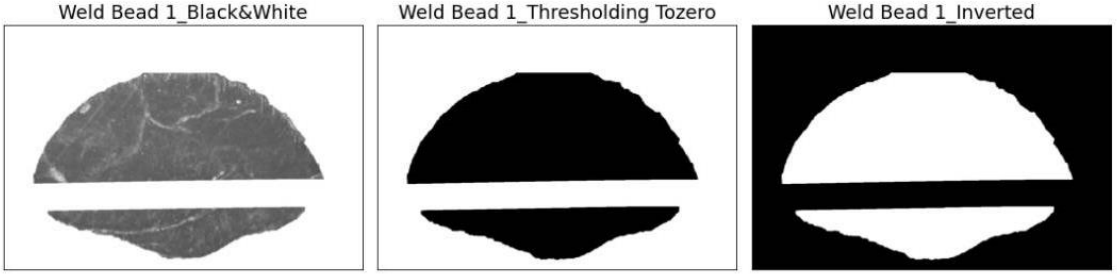

3) Find the contours

Using the function of Opencv: cv2.findcontours()

In [7]:
```
#Detect the contour of the weld bead
contours, hierarchy = cv2.findContours(WeldBead_gray_invert, cv2.RETR_TREE, cv2.CHAIN_APPROX_SIMPLE)[-2:]

#Draw the contour (red = 0,0,255) of weld bead in copied image
cv2.drawContours(WeldBead_copy, contours, -1, (0, 0, 255), 2)

#Show the result
plt.figure(figsize=[6,6])
plt.imshow(WeldBead_copy[:,:,::-1])
plt.title("Contours Detected = " +  str(len(contours)), fontsize= 18, y=0.9)
plt.axis("off");
```

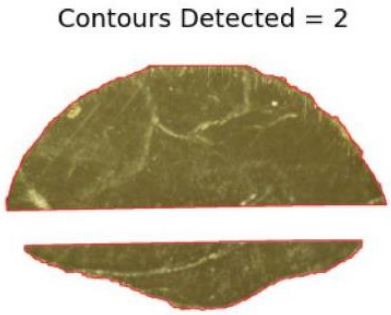

4) Calculation of A1 and A2

In [8]:
```
#Calculate the areas

biggest_contour = max(contours, key=cv2.contourArea)
smallest_contour = min(contours, key=cv2.contourArea)

A1= cv2.contourArea(biggest_contour)
A2 = cv2.contourArea(smallest_contour)

#Display Results
print("A1 = ", A1)
print("A2 = ", A2)
```

```
A1 =  292551.0
A2 =  99478.0
```

5) Calculate the Dilution Percentage

(Dilution = $\frac{A2}{A1+A2} * 100$ [%])

In [9]:
```
#Dilution Calculation
Dilution = (A2/(A1+A2))*100

#To Present in image which is A1 and which is A2 was used the function sorted to ordenate Contours
#The contours were sort in decreasing order
sorted_contours = sorted(contours, key=cv2.contourArea, reverse= True)

#Draw area A1 & A2
for i, cont in enumerate(sorted_contours[:2],1):
   #Display the position of contours in sorted list
    cv2.putText(WeldBead_copy, "A" + str(i), (cont[0,0,0], cont[0,0,1]-15), cv2.FONT_HERSHEY_COMPLEX, 2, (0,0,255)

#Display the Final Result
plt.figure(figsize=[6,6])
plt.imshow(WeldBead_copy[:,:,::-1]) #Present the original photo in original colours
plt.suptitle("WeldBead 1", x=0.51, y=0.82, fontsize= 15, fontweight="bold")
plt.title( "A1 = "+ str(A2) + "    A2 = "+  str(A2) + "   Dilution = "+  str(round(Dilution, 2))+  "%", y=0.9)
plt.axis("off")
plt.tight_layout();
```

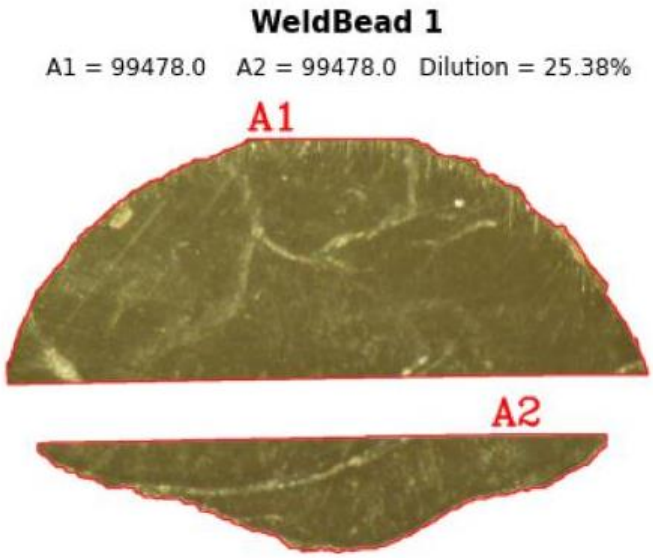
WeldBead 1
A1 = 99478.0 A2 = 99478.0 Dilution = 25.38%
A1
A2